Depositional and diagenetic variability within the Cambrian Mount Simon Sandstone: Implications for carbon dioxide sequestration

Brenda B. Bowen, Raul I. Ochoa, Nathan D. Wilkens, James Brophy, Thomas R. Lovell, Nick Fischietto, Cristian R. Medina, and John A. Rupp

ABSTRACT

The Cambrian Mount Simon Sandstone is the major target reservoir for ongoing geologic carbon dioxide (CO_2) sequestration demonstrations throughout the midwest United States. The potential CO_2 reservoir capacity, reactivity, and ultimate fate of injected CO_2 depend on textural and compositional properties determined by depositional and diagenetic histories that vary vertically and laterally across the formation. Effective and efficient prediction and use of the available pore space requires detailed knowledge of the depositional and diagenetic textures and mineralogy, how these variables control the petrophysical character of the reservoir, and how they vary spatially. Here, we summarize the reservoir characteristics of the Mount Simon Sandstone based on examination of geophysical logs, cores, cuttings, and analysis of more than 150 thin sections. These samples represent different parts of the formation and depth ranges of more than 9000 ft (>2743 m) across the Illinois Basin and surrounding areas. This work demonstrates that overall reservoir quality and, specifically, porosity do not exhibit a simple relationship with depth, but vary both laterally and with depth because of changes in the primary depositional facies, framework composition (i.e., feldspar concentration), and diverse diagenetic modifications. Diagenetic processes that have been significant in modifying the reservoir include formation of iron oxide grain coatings, chemical compaction, feldspar precipitation and dissolution, multiple generations of quartz overgrowth cementation, clay mineral precipitation, and iron oxide cementation. These variables provide important inputs for calculating CO_2 capacity potential,

DOI:10.1306/eg.07271010012

AUTHORS

BRENDA B. BOWEN ~ *Purdue University, West Lafayette, Indiana 47907; bbowen@purdue.edu*

Brenda B. Bowen is an assistant professor in the Department of Earth and Atmospheric Sciences at Purdue University. She received her B.S. and M.S. degrees in earth science from the University of California, Santa Cruz, and her Ph.D. in geology from the University of Utah in 2005. Her research is focused on understanding depositional and diagenetic processes that influence reservoir characteristics and paleoenvironmental records.

RAUL I. OCHOA ~ *Purdue University, West Lafayette, Indiana 47907*

Raul I. Ochoa is an M.S. student at Purdue University, studying reservoir characterization and diagenetic analysis of the Mount Simon Sandstone in the Illinois Basin related to geologic CO_2 sequestration. He received his B.S. degree from the University of Texas at El Paso in geology in 2008.

NATHAN D. WILKENS ~ *Purdue University, West Lafayette, Indiana 47907*

Nathan D. Wilkens is a postdoctoral research associate in the Department of Earth and Atmospheric Sciences at Purdue University. He earned his B.S. degree in geology in 2003 and a Ph.D. in geological sciences from Arizona State University in 2008. His research emphasis has been on depositional environments and paleoecology of terrestrial environments.

JAMES BROPHY ~ *Indiana University, Bloomington, Indiana 47405*

James Brophy is an associate professor of igneous petrology at Indiana University. His research specializes in the origin and differentiation of magma and uses a combination of field, analytical, theoretical, and experimental approaches. An important component of his work is the characterization of rock texture, mineralogy, and mineral composition through the application of petrographic and electron microprobe analytical techniques.

THOMAS R. LOVELL ~ *Purdue University, West Lafayette, Indiana 47907*

Thomas R. Lovell is a Ph.D. student at Purdue University, studying interactions between provenance and overall reservoir development in the Mount Simon Sandstone. He completed his M.S. thesis research at the University of Alabama while studying detrital zircon geochronology of an Early Jurassic reservoir in the Gulf of Mexico and his B.S. degree at the University of Tennessee-Chattanooga.

Nick Fischietto Purdue University, West Lafayette, Indiana 47907

Nick Fischietto received a B.S. degree from Allegheny College with a major in geology and an M.S. degree from Purdue University in geologic sciences, with a focus on clastic sedimentology. He is now working in the oil and gas industry in Oklahoma City.

Cristian R. Medina Indiana Geological Survey, Bloomington, Indiana 47405; present ddress: Indiana University, Bloomington, Indiana 47405

Cristian R. Medina is a reservoir geologist at the Indiana Geological Survey at Indiana University, Bloomington. He earned his B.S. degree in geology at the University of Chile in 2001 and his M.S. degree in hydrogeology at Indiana University, Bloomington, in 2007. He currently works for Midwest Regional Carbon Sequestration Partnership on the subsurface characterization of Cambrian sandstones.

John A. Rupp Indiana Geological Survey, Bloomington, Indiana 47405

John A. Rupp is a senior research scientist in the Subsurface Geology Section of the Indiana Geological Survey and associate director for science at the Center for Research on Energy and the Environment at Indiana University. He received his M.S. degree from Eastern Washington University in 1980, with emphasis on porphyry molybdenum deposits. Before joining the survey, he worked for Exxon Production Co. U.S.A. and for Salisbury and Dietz, Inc.

ACKNOWLEDGEMENTS

Funding sources included the U.S. Department of Energy; Midwest Geological Sequestration Consortium funded by the U.S. Department of Energy through the National Energy Technology Laboratory (NETL) via the Regional Carbon Sequestration Partnership Program (contract no. DE-FC26-05NT42588) and by a cost share agreement with the Illinois Department of Commerce and Economic Opportunity, Office of Coal Development through the Illinois Clean Coal Institute; the Midwest Regional Carbon Sequestration Partnership, managed by Battelle, with funding from the U.S. Department of Energy and other sponsors; and ExxonMobil. We thank collaborators at the Indiana Geological Survey and the Illinois State Geological Survey and David Barnes, David Morse, and an anonymous reviewer for thoughtful comments that helped improve the manuscript.

modeling reactivity, and are also an important baseline for comparisons after CO_2 injection.

INTRODUCTION

Increasing atmospheric carbon dioxide (CO_2) concentrations and their potential to affect global climate have led to extensive research and demonstrations of proposed methods for CO_2 sequestration. With an estimated storage capacity of as much as 1000 GT of CO_2 worldwide, deep saline reservoirs have the potential to make a significant contribution to reducing the amount of CO_2 emitted into the atmosphere in the coming decades (Holloway, 2001; Kharaka et al., 2006; Benson and Cole, 2008). Geologic sequestration presents a potential long-term method of CO_2 storage through trapping mechanisms, including buoyant, solubility, and capillary trapping and chemical fixation of CO_2 into mineral form in the subsurface. Realization of the estimated geologic sequestration storage potential will require detailed evaluations of sequestration regions and injection site localities at several different times during project life cycles. Initial identification of appropriate sequestration sites is based on the presence of reservoir facies, appropriate hydrodynamical setting, depth, the presence of an overlying impermeable seal, and a relative lack of structural discontinuities and seismic activity that could cause the reservoir or seal system to fail during operation (Leetaru and McBride, 2009). In addition to these factors, detailed reservoir rock characterization is a critical component of any specific CO_2 sequestration project. Such an examination provides a predictive framework for determining reservoir quality, generates data that serve as essential input values for fluid flow and geochemical modeling, and establishes a baseline for future assessments of how CO_2 will influence a reservoir after injection has occurred.

The Cambrian Mount Simon Sandstone is currently being targeted as a major potential CO_2 reservoir throughout the midwest United States (Leetaru et al., 2008; Barnes et al., 2009; Medina et al., 2011). The Mount Simon Sandstone unconformably overlies Precambrian crystalline basement and was deposited during the Late Cambrian in the proto-Illinois Basin, a broad cratonic basin that was open to the sea to the south (Kolata and Nelson, 1991; Fishman, 1997). The Mount Simon Sandstone is a member of the Potsdam Supergroup and is the lowermost member of the Sauk transgressive sequence in the Illinois Basin (Sloss, 1963). Outcrops of Mount Simon Sandstone exist in Minnesota, Wisconsin, and Iowa, and correlative units such as the Lamotte Sandstone and the Reagan Sandstone are exposed in Missouri, Oklahoma, Kansas, and Nebraska (Houseknecht and Ethridge, 1978; Driese et al., 1981). The Mount Simon Sandstone and its equivalents occur in the subsurface throughout much of the midwest and eastern states, with accumulations in Illinois and Indiana, ranging in thickness from zero in the southwest

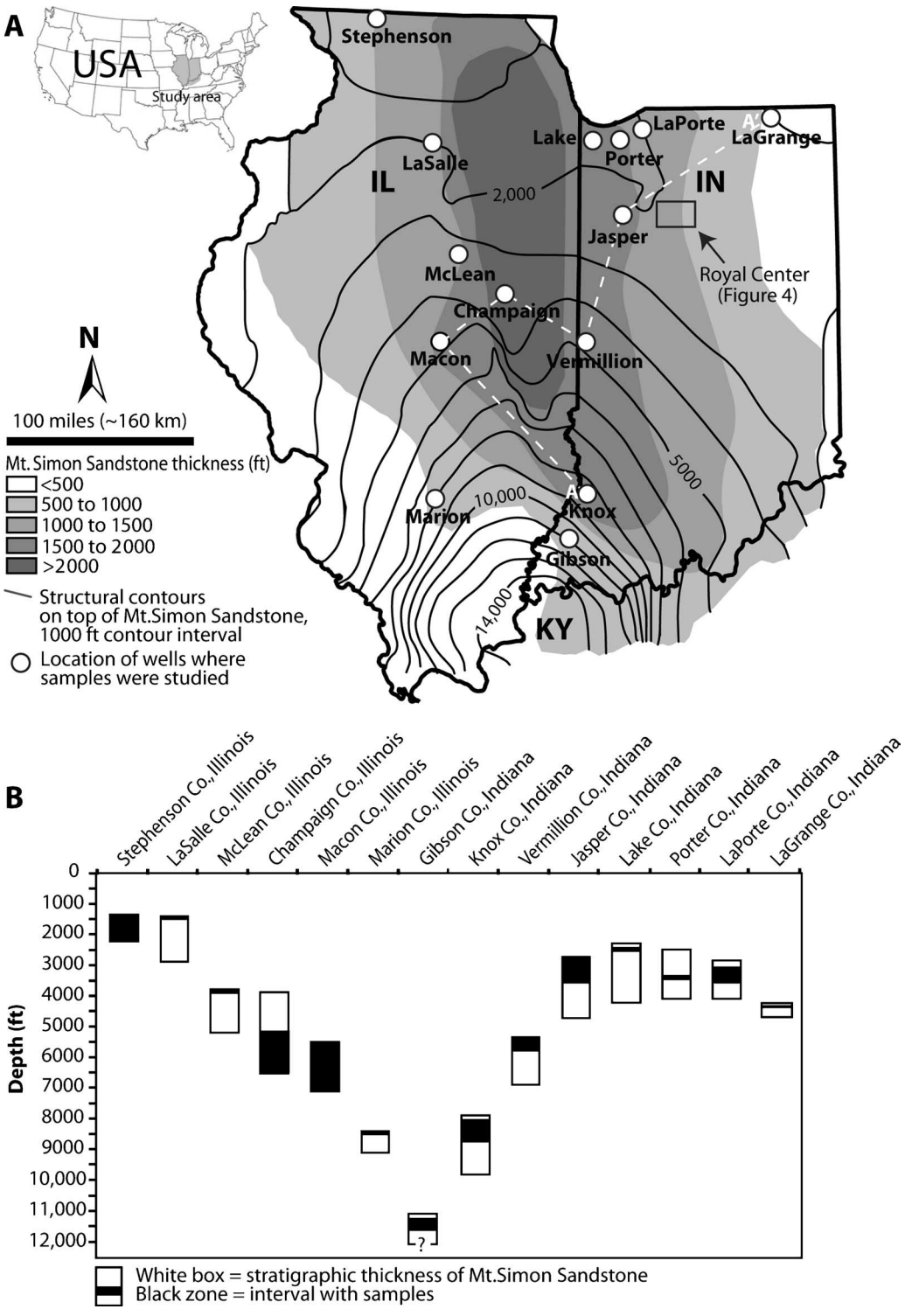

Figure 1. Location of Mount Simon Sandstone samples included in this study. (A) Map showing geographic location of sampled wells (identified by county). Well details listed in Table 1. Approximate thickness of the Mount Simon Sandstone and structure (burial depth) on top of the Mount Simon Sandstone (modified from Leetaru et al., 2008). AA′ shows location of cross section in Figure 3. Box labeled "Royal Center" shows area included in Figure 4. (B) Schematic cross section of sampled wells showing thickness and current depth of Mount Simon Sandstone (white box) and sampled interval (black zone within white box) that includes a mixture of sample types such as whole core, sidewall core, and/or thin sections. Thicknesses derived from well-log data. Wells ordered N-S through Illinois and then S-N through Indiana.

Illinois Basin to more than 2500 ft (~762 m) in the thickest part of the basin (Figure 1). The Mount Simon Sandstone is conformably overlain by the Upper Cambrian Eau Claire Formation, a unit composed of siltstone, shale, sandstone, and dolomite (Becker et al., 1978) that is identified as the primary seal for the basal sandstone CO_2 sequestration system in the midwest (Wickstrom et al., 2006; Leetaru et al., 2008).

Historically, only a limited number of wells in the Illinois Basin and surrounding areas penetrate the Mount Simon Sandstone, and an even smaller number of wells extend beyond the first few hundred feet of the

unit. Of those wells that penetrated a significant part of the Mount Simon Sandstone, only a very small number were extensively cored, and in fact, only one core is known that covers the entire formation in this region (Stephenson Co., Illinois) (Fischietto, 2009). Recent and ongoing sequestration research activities by the U.S. Department of Energy–supported Midwest Geologic Sequestration Consortium and Midwest Regional Carbon Sequestration Partnership have resulted in the drilling of multiple new wells that penetrate significant parts of the Mount Simon Sandstone. These new wells have expanded the amount of materials available for study and provide new opportunities for understanding the Cambrian depositional system and the diagenetic history of the Illinois Basin.

The ability to predict how CO_2 will behave in the subsurface relies, in part, on a detailed understanding of the composition of the geologic materials that make up the reservoir and seal on macroscopic to microscopic scales (Parry et al., 2007). Some of the potential risks with large-scale CO_2 injection and storage include possible dissolution of reactive minerals and geomechanical responses related to increases in fluid pressure (Friedmann, 2007). Field-based CO_2 injection projects, experimental projects, natural CO_2-charged analogs, and geochemical modeling demonstrate the range of complex geochemical interactions that occur among CO_2, formation water brines, and reservoir rocks. As supercritical CO_2 dissolves in formation brines, fluid pH can drop significantly, depending on the pressure and temperature of the formation water and the abundance of mineral buffers, such as calcite and aluminosilicates (Parry et al., 2007). The low pH can lead to dissolution of some primary phases and precipitation of subsequent secondary minerals (Kharaka et al., 2006; Wigand et al., 2008). Some possible reactions that could alter the porosity and permeability of the reservoir rock include dissolution of carbonate grains and cements, dissolution of iron oxide grain coatings, and alteration of feldspars.

The objective of this article is to provide an overarching summary of the dominant sedimentologic features that influence the quality of the Mount Simon Sandstone as a CO_2 reservoir in the Illinois Basin, including (1) the depositional facies and (2) the diagenetic modifications that have occurred more than the approximately 500 m.y. burial history. Here, we focus on how these factors influence porosity, composition, and texture, with an emphasis on the primary and secondary minerals that would potentially be reactive with possible geochemical changes in formation fluid chemistry because of CO_2 injection. We also identify areas for future research that will be important contributions as ongoing CO_2 sequestration projects targeting the Mount Simon Sandstone continue.

METHODS

Mount Simon Sandstone samples derived from whole cores, sidewall cores, and cuttings from 15 subsurface localities in the Illinois Basin in Indiana and Illinois were examined using a combination of descriptive, mineralogical, geochemical, and petrographic techniques (Table 1). These samples represent variable formation thicknesses, depositional facies, and burial depths (Figure 1). Samples investigated in this study range from minimum depths of about 1300 ft (~396 m) to maximum depths of more than 11,000 ft (3354 m). Cores were described in terms of sedimentologic textures, depositional features, and macroscopic diagenetic features (Figure 2). Cored and sampled zones were correlated, where possible, to available digital geophysical well logs from the Indiana Geological Survey and the Illinois State Geological Survey using the HIS-Petra software suite (Figure 3). Lithologic strip logs, created with well cuttings by the Indiana Geological Survey, were used to examine lateral variability in lithology and mineralogy of some closely spaced wells in northern Indiana (Royal Center) where core samples are not available (Figure 4).

All examined samples and well cuttings on the strip logs from the Royal Center Gas Project (location in Figures 1, 4) were analyzed using short-wave to near-infrared reflectance spectroscopy (using an Analytical Spectral Device FieldSpec3). This is a nondestructive analysis that can be used to qualitatively assess some aspects of mineralogy, particularly authigenic components in siliciclastic units (Clark, 1999; Bowen et al., 2007). Samples were illuminated with artificial light (a broadband DC light source), and spectral reflectance was measured on 2151 channels from 350 to 2500 nm. The area of a sample analyzed for each measurement was a circle with a diameter of 1 cm (0.3 in.). For the well-cutting strip logs, spectra were measured at 1-in. (2.5-cm) intervals, representing 20 ft (6 m) of drilled material. Quartz and feldspars have flat spectral reflectance curves in these wavelengths, making these analyses ideal for evaluating other minor minerals in quartzose to arkosic sandstones (Bowen et al., 2007).

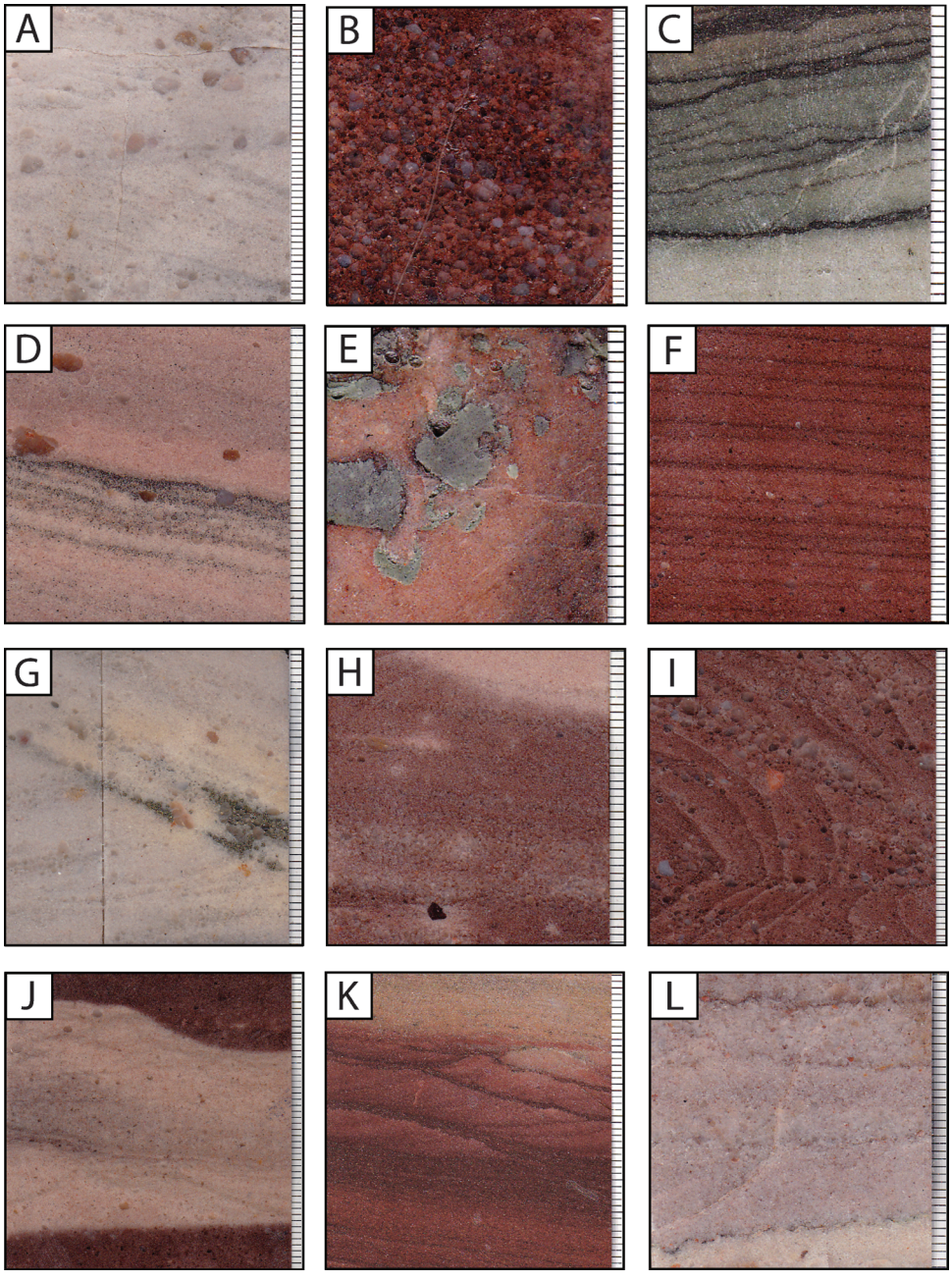

Figure 2. Core photographs showing typical colors and textures in the Mount Simon Sandstone (from well in Knox Co., Indiana). Panels A–F show typical depositional textures; panels G–L show typical diagenetic textures. Scale bars on right of each photo denote millimeters. (A) Poorly sorted coarse-grained cross-bedded sandstone with floating quartz granules, 8090 ft (2467 m). (B) Poorly sorted coarse-grained sandstone, 8633 ft (2632 m). (C) Interstatified shale and fine-grained sandstone, 8093 ft (2467 m). (D) Poorly sorted medium-grained cross-bedded sandstone, 8630 ft (2631 m). (E) Poorly sorted fine-grained sandstone with mudstone rip-up clasts, 8642 ft (2635 m). (F) Interstratified shale and medium- to coarse-grained sandstone, 8842 ft (2696 m). (G) Poorly sorted cross-bedded sandstone with pyrite cement, 8090 (2467 m). (H) Poorly sorted cross-bedded sandstone with isolated reduction spots (white) within red sandstone, 8630 ft (2631 m). (I) Poorly sorted cross-bedded sandstone with liesegang banding cutting across bedding, 8631 ft (2631 m). (J) Poorly sorted fine-grained cross-bedded sandstone with reduction zone sandwiched between red oxidized zones, 8641 ft (2634 m). (K) Interstratified shale and medium- to coarse-grained sandstone with gradational liesegang banding between iron oxide–rich and iron oxide–poor zones, 8651 ft (2638 m). (L) Poorly sorted cross-bedded medium-grained sandstone with stylolitic chemical compaction texture (dark irregular lines), 8841 ft (2695 m).

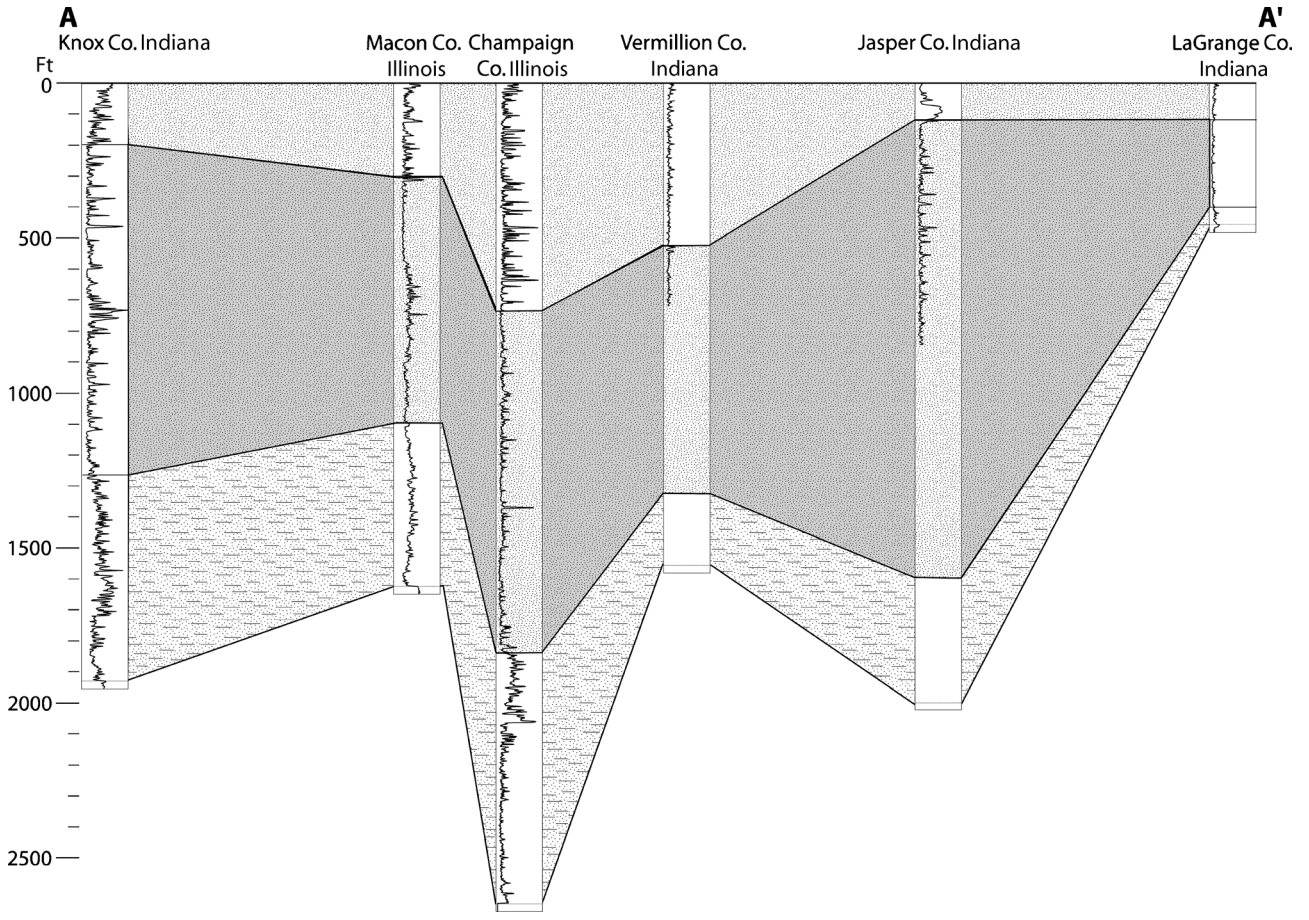

Figure 3. Stratigraphic cross section of Mount Simon Sandstone from petrophysical well logs (gamma-ray). AA' approximately south to north across the Illinois Basin. Wells shown are some of those where samples were examined in this study (note that not all wells have complete well-log data available). Cross section is hung on the top of the Mount Simon Sandstone and continues down to the Precambrian basement. The three-part subdivision (Medina and Rupp, 2010) is based on defining (1) an upper unit that has relatively high gamma-ray values (generally >75 API) because of the admixture of argillaceous material. In some parts of northern Indiana, this upper unit can be further subdivided into an upper sand unit and a lower shale unit (also known as the "B-Cap," Becker et al., 1978), which may serve as a secondary seal below argillaceous horizons in the overlying Eau Claire Formation; (2) a middle unit defined by lower gamma-ray values (<75 API) that result from a cleaner quartzose sandstone and potentially constitutes the main reservoir and flow unit within the formation. The gamma-ray values of this unit also display the lowest amount of vertical variability through the section, and (3) a lowermost unit defined by gamma-ray values that progressively increase with depth to the base of the formation (>75 API). This downward increase is caused by an increase in the nonquartz fraction with depth.

Diagnostic spectral absorption features allow for identification of the presence or absence of some minerals including iron oxides, carbonates, sulfates, illite-group clays, and kaolinite (Clark, 1999). The depth of mineral-specific absorption features generally correlates with mineral abundance (as well as other parameters including grain size), allowing for a semiquantitative assessment of the abundance of select minerals (Figure 4). Relative abundances are compared by calculating and comparing the depths of absorption features in continuum removed spectra (Clark and Roush, 1984). Because of the complex nonlinear nature of spectral reflectance data in these wavelengths, it is not possible to assign a quantitative scale to these data.

Approximately 150 thin sections from 14 different wells (Figure 1) were prepared from whole-core and sidewall core samples and qualitatively analyzed using standard petrographic methods and cathodoluminescence (CL) microscopy. Thin sections were impregnated with blue epoxy under vacuum to identify porosity and were stained with sodium cobaltinitrite for identification of K-feldspar. Compositions (primary framework grains, secondary minerals, and porosity) were quantified using standard point-counting methods

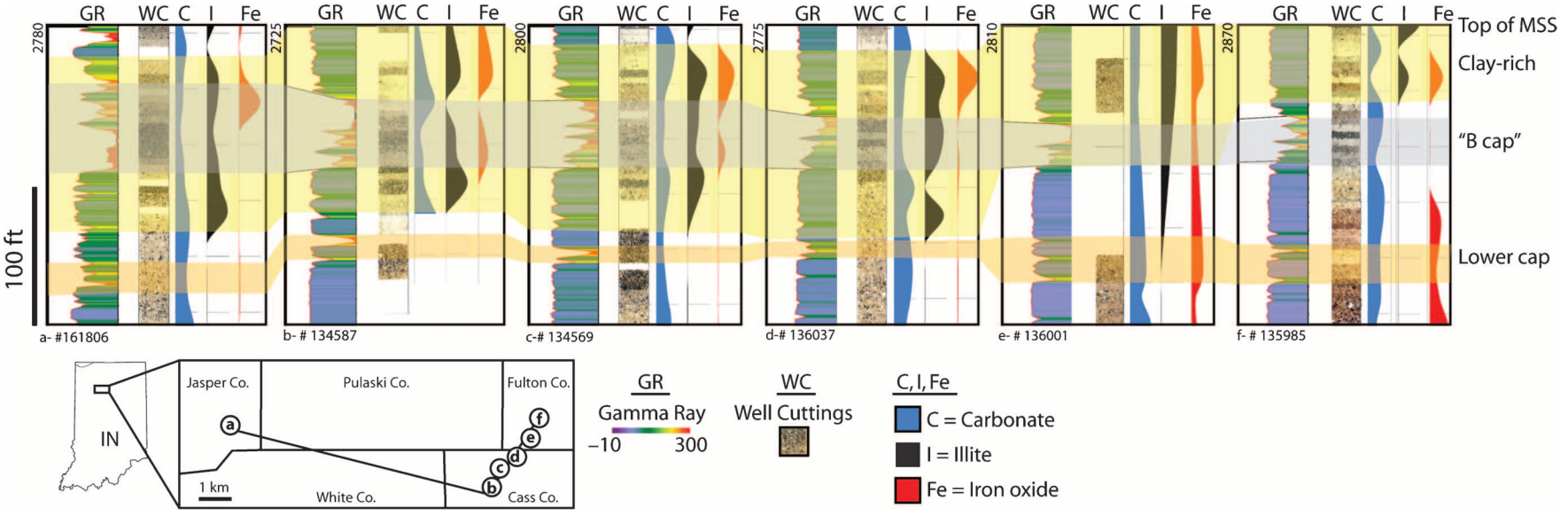

Figure 4. Stratigraphic cross section illustrating the compositional variability in the upper 200 ft (61 m) of the Mount Simon Sandstone in six closely spaced wells northwestern Indiana at the Royal Center Gas Storage Project (see Figure 1 for location). Well numbers shown at base. Data in cross section include gamma-ray geophysical well logs (see color ramp with gamma-ray values; yellow, orange, and red suggest high content of nonquartz [e.g., argillaceous] material, and blue and green suggest "clean" sandstone), photographs of well-cuttings strip logs (strip logs supplied by the Indiana Geological Survey), and semiquantitative mineral abundance data (carbonate, illite, and iron oxide) determined from reflectance spectroscopy (see text for details on method). Datum = top of Mount Simon Sandstone (depths of formation top at individual wells shown on upper left in feet).

Table 1. Well Identification Information*

County, State	Well Name	ID No.
Stephenson Co., Illinois	UPH 3	121772131700 (API)
LaSalle Co., Illinois	Mathesius L 1	120990103800 (API)
McLean Co., Illinois	Brokaw 5	121132195600 (API)
Champaign Co., Illinois	Hinton Brothers 7	120192399601 (API)
Macon Co., Illinois	ADM CCS Well 1	121152341500 (API)
Marion Co., Illinois	Johnson RS 1	121210519800 (API)
Lake Co., Indiana	U.S. Steel WD 1	142097 (IGS)
LaPorte Co., Indiana	Criterion Catalyst WD 1	159265 (IGS)
Porter (1) Co., Indiana	Midwest Steel WD 1	144461 (IGS)
Porter (2) Co., Indiana	Stoltemberg Const. Co. WD 1	144409 (IGS)
LaGrange Co., Indiana	L and R Inc	159232 (IGS)
Jasper Co., Indiana	H and L Boezman 1	162029 (IGS)
Vermillion Co., Indiana	Newport Chem WD 1	125110 (IGS)
Knox Co., Indiana	Duke Energy IGCC 1	NA**
Gibson Co., Indiana	Duke 2 Gibson Station	NA

*Information on subsurface wells where Mount Simon Sandstone was sampled and investigated for this study. Table includes county, state, well name, API identification number, or IGS identification number (Indiana Geological Survey identification number for wells in Indiana).
**NA = not available (wells that have not yet been assigned with an identification number).

(typically 500 points per thin section) on representative samples derived from sidewall cores that span the entire depth of the formation and include two densely sampled 30-ft (9-m) sections of whole core from the well in Macon Co., Illinois (n = 62 thin sections; Table 2).

The amount of porosity visible in thin section was identified and quantified from digital micrographs of 91 thin sections from seven different wells (Stephenson Co., Illinois; Champaign Co., Illinois; Macon Co., Illinois; Marion Co., Illinois; Knox Co., Indiana; Jasper Co., Indiana; and LaGrange Co., Indiana). Porosity was quantified using a maximum likelihood algorithm within ITT Visual Information Solutions ENVI digital imaging software (Figure 5). The maximum likelihood algorithm is based on defining pixels that are known to be porosity (defining at least 15,000 porosity pixels) and then applying the classification to the entire micrograph where pixels with an 80% similarity or greater are also classified as porosity. The average porosity from four micrographs at 20× magnification (and six micrographs at 100× magnification for a subset of samples) was quantified per thin section to get an overall representative visible percent porosity.

Relative percents of pore linings occupied by quartz or feldspar were determined on 25 thin sections using backscattered electron (BSE) images in conjunction with the National Institutes of Health image analysis software program (ImageJ). The BSE images were used to delineate quartz, feldspar, and open-pore space in terms of gray scale. The images were calibrated so that the number of pixels could be correlated to true area. Pore-space maps were created, and perimeter lengths of individual pores were measured. The length of individual pore-space perimeter that was made up of feldspar was used to determine the relative percentage of feldspar lining pore perimeters. Select representative samples were also analyzed for mineralogy with x-ray diffraction (n = 15). Whole-rock geochemistry (major oxides and trace elements) was determined on a representative suit of samples from Stephenson Co., Illinois, and Jasper Co., Indiana (n = 51), by Activation Laboratories using inductively coupled plasma–mass spectroscopy (Table 2).

DEPOSITIONAL FACIES AND SEDIMENTARY ENVIRONMENTS

The Mount Simon Sandstone is commonly referred to as a "sheet sandstone" due to its laterally extensive siliciclastic nature, but heterogeneity within cores or between wells demonstrates that it does not have a simple sheet-like geometry (Figures 3, 4). Irregular steep-sided horst and graben topography on the underlying Precambrian crystalline basement shows as much as 1800 ft (549 m) of relief, creating isolated and petrologically distinct subbasins (Leetaru and McBride, 2009; Houseknecht and

Table 2. Whole-Rock Geochemical Analyses for the Mount Simon Sandstone

Well (county)	Depth (ft)	Sed Description*	Color	SiO_2	Al_2O_3	Fe_2O_3(T)	MnO	MgO	CaO	Na_2O	K_2O	TiO_2	P_2O_5	LOI	Total	Ba	Sr	Y	Sc	Zr	Be	V
Jasper Co., Indiana	2821	f ss	White	97.04	1.47	1.46	0.011	0.11	0.03	0.04	0.64	0.064	0.03	0.12	101	50	49	10	<1	54	<1	6
Jasper Co., Indiana	2848	f-m ss	Red	92.4	3.21	1.88	0.013	0.05	0.08	<0.01	2.92	0.186	0.08	–0.12	100.7	430	66	10	2	351	<1	6
Jasper Co., Indiana	2900	mixed shale and f ss	Gray	89.08	3.55	1.49	0.015	0.13	0.66	0.07	2.61	0.181	0.57	0.65	99.01	113	109	39	3	136	<1	17
Jasper Co., Indiana	2949	c ss	Red	97.15	0.86	0.83	0.005	0.02	0.05	0.03	0.65	0.052	0.04	–0.01	99.68	91	30	3	<1	37	<1	<5
Jasper Co., Indiana	2960	f ss	Green	98.07	0.48	1.51	0.009	0.02	0.03	<0.01	0.43	0.058	0.02	–0.22	100.3	57	22	2	2	82	<1	7
Jasper Co., Indiana	3015	c ss	White	75.03	11.73	2.12	0.013	0.78	0.08	0.28	6.11	0.766	0.07	2.12	99.1	737	255	20	11	393	2	85
Jasper Co., Indiana	3024	mixed shale and f ss	Green	95.28	2.27	1.45	0.009	0.08	0.04	<0.01	1.35	0.123	0.03	0.22	100.8	224	76	2	1	80	<1	<5
Jasper Co., Indiana	3070	f ss	White	95.19	1.53	1.42	0.009	0.04	0.57	<0.01	0.52	0.111	0.02	1.18	100.5	39	43	1	2	135	<1	8
Jasper Co., Indiana	3086	c ss	Red	96.59	0.76	1.49	0.009	0.02	0.04	<0.01	0.47	0.159	0.02	0.06	99.54	76	49	<1	2	181	<1	12
Jasper Co., Indiana	3180	f-m ss	Green	91.25	3.91	1.17	0.009	0.14	0.05	<0.01	1.99	0.182	0.02	0.46	99.17	233	52	7	3	287	<1	13
Jasper Co., Indiana	3225	f ss	Red	54.24	24.27	7.8	0.012	0.56	0.07	0.2	4.49	1.262	0.11	6.71	99.74	211	335	26	20	572	3	362
Jasper Co., Indiana	3311	m ss	White	93.89	0.54	1.06	0.009	0.02	1.43	<0.01	0.23	0.055	<0.01	2.47	99.69	48	49	2	<1	100	<1	<5
Jasper Co., Indiana	3365	c ss	White	96.76	0.69	1.16	0.009	0.02	0.08	<0.01	0.51	0.068	0.02	0.05	99.36	91	27	<1	2	84	<1	7
Jasper Co., Indiana	3396	ms	Red and green	76.42	12.43	1.65	0.008	0.53	0.16	0.2	6.07	0.973	0.06	2.29	100.8	554	208	29	8	1329	<1	61
Jasper Co., Indiana	3420	m-c ss	White	95.38	1.56	1.08	0.009	0.07	0.05	<0.01	0.89	0.14	0.04	0.22	99.65	119	77	3	1	123	<1	<5
Jasper Co., Indiana	3484	m ss	White	92.79	3.54	1.44	0.009	0.18	0.07	<0.01	1.75	0.441	0.05	0.61	100.9	186	105	8	3	242	<1	15
Jasper Co., Indiana	3526	m-c ss	White	96.43	1.11	1.31	0.01	0.04	0.11	0.11	0.65	0.085	0.02	0.18	100	230	150	2	<1	88	<1	<5
Jasper Co., Indiana	3604	m-c ss	White	94.03	1.74	1.4	0.011	0.05	0.05	0.16	1.19	0.525	0.02	0.21	99.39	173	62	5	<1	165	<1	6
Jasper Co., Indiana	3657	m-c ss	White	96.53	0.8	1.3	0.01	0.02	0.04	0.08	0.56	0.056	0.02	–0.18	99.25	78	41	1	<1	43	<1	<5
Stephenson Co., Illinois	1308	c ss	Red	95.5	0.78	1.89	0.008	0.12	0.1	0.04	0.44	0.048	0.02	0.23	99.17	35	14	2	<1	76	<1	23
Stephenson Co., Illinois	1327	m-c ss	Red	93.52	2.45	1.12	0.004	0.29	0.05	<0.01	1.22	0.179	0.03	0.61	99.61	78	30	12	2	156	<1	37
Stephenson Co., Illinois	1339	f ss	Green	95.81	1.01	0.8	0.005	0.09	0.02	0.01	0.62	0.056	0.02	0.13	98.57	33	12	2	<1	67	<1	14
Stephenson Co., Illinois	1359	f ss	Red	96.74	1.2	1.23	0.008	0.1	0.06	<0.01	0.72	0.074	0.03	0.04	100.2	51	13	2	2	83	<1	15
Stephenson Co., Illinois	1368	m-c ss	Green	97.61	0.83	0.99	0.009	0.1	0.21	<0.01	0.44	0.065	0.16	0.09	100.4	39	12	2	2	72	<1	14
Stephenson Co., Illinois	1425	c-granular ss	White	99.88	0.26	0.69	0.004	<0.01	0.03	<0.01	0.23	0.051	0.02	–0.11	101	32	14	2	2	63	<1	5
Stephenson Co., Illinois	1451	f ss	Red	67.05	12.51	3.58	0.02	0.68	3.19	0.13	7.92	0.615	2.51	1.96	100.2	940	220	43	9	258	3	110
Stephenson Co., Illinois	1474	m-c ss	White	98.27	0.52	0.62	0.005	0.02	0.04	0.04	0.33	0.07	0.04	–0.01	99.95	44	32	3	<1	89	<1	<5
Stephenson Co., Illinois	1492	f ss	White	96.04	0.52	2.51	0.015	0.05	0.04	<0.01	0.12	0.052	0.03	–0.48	100.8	29	17	<1	<1	71	<1	<5
Stephenson Co., Illinois	1514	m-c ss	White	98.09	0.77	1.04	0.008	0.05	0.02	0.01	0.29	0.033	0.02	0.01	100.3	18	10	2	<1	34	<1	<5
Stephenson Co., Illinois	1552	c-granular ss	Red	97.58	0.73	1.11	0.007	0.03	0.03	<0.01	0.18	0.088	0.04	0.01	99.73	21	40	3	1	126	<1	<5
Stephenson Co., Illinois	1590	m ss	White	96.74	1.95	1.29	0.008	0.07	0.02	<0.01	0.61	0.065	0.03	0.21	100.9	23	45	1	2	74	<1	8

Stephenson Co., Illinois	1631	c-granular ss	Red	98.08	0.76	1.13	0.008	0.04	0.02	<0.01	0.23	0.063	0.03	0.05	100.3	19	35	4	2	82	<1	10
Stephenson Co., Illinois	1672	c ss	Red	95.95	0.73	2.79	0.018	0.05	0.02	<0.01	0.22	0.025	0.03	−0.42	99.3	18	41	2	1	41	<1	<5
Stephenson Co., Illinois	1693	ms	Red	86.7	6.04	2.42	0.011	0.37	0.05	0.01	1.88	0.288	0.04	1.31	99.12	39	111	11	2	267	2	34
Stephenson Co., Illinois	1699	c-granular ss	Red	91.5	1.3	3.02	0.018	0.11	0.52	<0.01	0.36	1.716	0.43	0.12	99	34	123	29	3	1003	<1	57
Stephenson Co., Illinois	1726	c ss	Red	95.95	0.98	1.38	0.013	0.13	0.14	<0.01	0.21	0.057	0.06	−0.01	98.78	18	46	2	2	63	<1	<5
Stephenson Co., Illinois	1763	c ss	Red	97.21	1.06	2	0.009	0.09	0.07	<0.01	0.35	0.036	0.04	0.07	100.8	22	118	2	1	42	<1	9
Stephenson Co., Illinois	1775	c ss	Red	94.99	1.9	1.25	0.009	0.19	0.06	<0.01	0.72	0.05	0.03	0.32	99.51	24	43	4	2	80	<1	7
Stephenson Co., Illinois	1801	m ss	Red	94.77	1.31	1.69	0.014	0.1	0.03	<0.01	0.56	0.031	0.03	0.03	98.5	18	25	<1	<1	50	<1	<5
Stephenson Co., Illinois	1813	c-granular ss	White	88.09	5.35	1.73	0.009	0.65	0.09	<0.01	2.1	0.487	0.04	1.18	99.69	48	101	17	5	526	<1	24
Stephenson Co., Illinois	1856	m ss	Red	95.68	1.44	1.83	0.014	0.16	0.04	<0.01	0.77	0.111	0.03	0.1	100	18	42	5	2	85	<1	6
Stephenson Co., Illinois	1885	ms	Red	48.69	24.25	9.88	0.004	2.45	0.14	0.03	7.69	1.265	0.13	6.28	100.8	242	449	76	14	389	9	139
Stephenson Co., Illinois	1919	c ss	Red	96.94	0.64	1.49	0.015	0.04	0.09	0.03	0.4	0.03	0.07	−0.08	99.67	6	18	7	<1	59	<1	7
Stephenson Co., Illinois	1948	m ss	Red	97.34	0.71	1.78	0.014	0.04	0.49	<0.01	0.54	0.03	0.03	0.03	100.9	17	18	6	1	69	<1	<5
Stephenson Co., Illinois	2012	m ss	Red	98.21	0.61	1.4	0.01	0.03	0.03	0.03	0.4	0.023	0.03	−0.16	100.6	4	18	5	<1	30	<1	<5
Stephenson Co., Illinois	2037	f ss	Red	94.9	1.89	1.25	0.008	0.17	0.03	0.01	0.98	0.056	0.03	0.3	99.62	9	29	5	<1	69	<1	<5
Stephenson Co., Illinois	2054	m ss	Red	94.59	1.75	2.16	0.008	0.2	0.03	0.01	1.1	0.055	0.03	0.12	100.1	10	36	7	<1	55	<1	7
Stephenson Co., Illinois	2062	c ss	Red	96.87	0.81	1.79	0.011	0.05	0.08	<0.01	0.6	0.106	0.02	−0.05	100.3	265	24	9	<1	66	<1	<5
Stephenson Co., Illinois	2085	c-granular ss	Red	95.97	1.01	1.94	0.008	0.1	0.01	0.01	0.7	0.044	0.02	0.02	99.85	10	22	8	<1	43	<1	9
Stephenson Co., Illinois	2105	c ss	Red	97.33	0.86	2.16	0.013	0.1	0.03	<0.01	0.56	0.045	0.03	−0.28	100.7	18	22	10	<1	84	<1	<5
Stephenson Co., Illinois	2142	c ss	White	98.67	0.49	1.44	0.009	0.03	0.02	<0.01	0.42	0.032	0.03	−0.17	100.9	17	26	15	1	74	<1	<5

*ms = mudstone; f ss = fine grained sandstone; f-m ss = fine to medium grained sandstone; m ss = medium grained sandstone; m-c ss = medium to coarse grained sandstone; c ss = coarse sandstone; c-granular ss = coarse to granular sandstone.

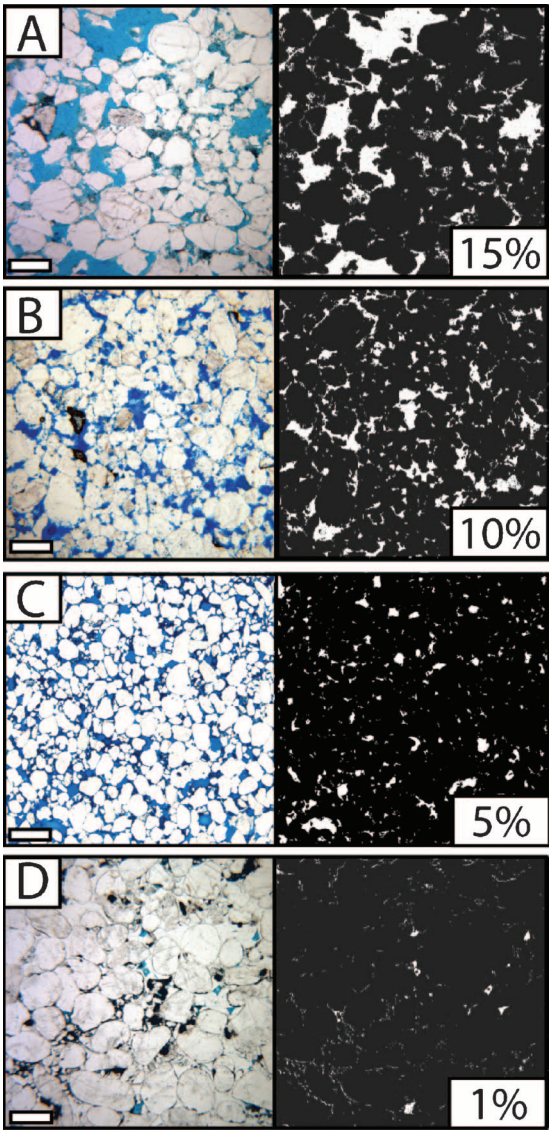

Figure 5. Examples of petrographic image classification of porosity in the Mount Simon Sandstone. Micrographs (transmitted plane light) left (blue epoxy = porosity) with porosity classification on right (white = porosity). Scale bars = 1 mm. (A) Mixed intergranular and secondary dissolution porosity, 15% porosity (Stephenson Co., 1845 ft [560 m]). (B) Intergranular and intragranular porosity, 10% porosity (Jasper Co., 4309 ft [1305 m]). (C) Intergranular porosity, 5% porosity (Macon Co., 6060 ft [1848 m]). (D) Quartz-cemented sample with only 1% porosity (Marion Co., 8468 ft [2566 m]).

Ethridge, 1978). Depositional environments interpreted in the formation range from shallow-marine, deltaic, and fluvial systems to eolian and potentially sabkha settings (Driese et al., 1981; Hagadorn et al., 2002; Fischietto, 2009). Regional correlation of lithofacies in the Mount Simon Sandstone shows that the fine-grained interbeds cannot be correlated across wells (Figure 4). For regional analyses, a three-part subdivision of petrofacies (e.g., Medina and Rupp, 2010) corresponds to the changes in lithology observed in samples (Figure 3). Although large-scale trends in lithology are documented regionally (Barnes et al., 2009), close examination of specific wells reveals variations in depositional textures and composition both laterally and with depth. However, a detailed examination of spatial patterns in depositional facies is beyond the scope of this article.

Primary sedimentary facies in the Mount Simon Sandstone were defined based on the examination of four cores (Stephenson Co., Illinois; Knox Co., Indiana; Jasper Co., Indiana; and Vermillion Co., Indiana) and synthesis with published literature based on outcrops in Wisconsin and Missouri (Houseknecht and Ethridge, 1978; Driese et al., 1981). We observe six dominant lithofacies within the Mount Simon Sandstone that have variable diagenetic alteration and fossil occurrence (Figure 2). These six lithofacies include (1) cobble conglomerate, (2) stratified gravel conglomerate, (3) poorly sorted sandstone, (4) well-sorted sandstone, (5) interstratified sandstone and shale, and (6) shale. The cobble conglomerate facies is a matrix-supported massive deposit composed of gravel- to boulder-size clasts of locally derived basement material. These deposits occur at the Mount Simon Sandstone–Precambrian contact and are especially common in Missouri (Ojakangas, 1963) and southern Illinois (Leetaru and McBride, 2009). The stratified gravel conglomerate facies is a planar bedded to tabular cross-bedded poorly sorted sandstone and gravel conglomerate. It is composed of medium sand to pebble-size grains that are normally graded with gravel and sand beds. Some granule- to pebble-size clasts of feldspar in this facies are visibly altered to clay. The poorly sorted sandstone facies is a massive to tabular cross-bedded sandstone with poorly sorted medium to coarse sand. This facies contains *Skolithos* vertical trace fossils in the middle and upper part of the Mount Simon Sandstone. This is the most common lithofacies throughout the Mount Simon Sandstone (Figure 2). The well-sorted sandstone facies is a medium- to fine-grained quartz sandstone that is commonly cross bedded. This facies is relatively rare and is found in isolated zones in the middle of the Mount Simon Sandstone. The interstratified sandstone and shale facies contains distinct sets of silt to sand planar beds interspersed with thin shale beds and rare dewatering or soft-sediment deformation structures. *Planolites* trace fossils are found in this facies in the uppermost Mount Simon Sandstone. Finally, the shale facies is

dominated by massive to thin-bedded mudstone with lenticular bedding similar to the interstratified sandstone and shale lithofacies. This facies is most common in the upper part of the 401 Mount Simon Sandstone. Sand and silt interbeds in this facies contain *Planolites* trace fossils and transported assemblages of calcium phosphate shells of the inarticulate brachiopod *Obolus*. This lithofacies contains thick zones of shale with silt and sand that have distinctive vertical features with as much as 2 cm (0.7 in.) of relief, in addition to rare mud cracks. The vertical features are typically V-shape in cross section, mostly pointing downward with some pointing upward and are commonly ptygmatically folded. In plan view, they are many times wider than tall, with random patterns and orientations. These enigmatic vertical features represent soft-sediment deformation formed from injection of liquidized material into overlying sediments possibly formed during rapid dewatering related to seismic activity (Pratt, 1998).

Paleoenvironmental interpretations are complicated by the existence of regionally variable basement topography, together with wide and very low angle shelves in the Precambrian and early Paleozoic. The shelf deposits are difficult to discern from continental orthoquartzite successions (Cant and Hein, 1986; Dott et al., 1986; Soegaard and Eriksson, 1989). Instead, body and trace fossils are used to constrain marine environments because the earliest freshwater trace fossils do not occur until the Upper Ordovician (Lehmann et al., 2001; Tomescu, 2004). By the Early Cambrian, widespread marine animals (metazoans) were burrowing at the decimeter scale into near-shore sands (Droser and Bottjer, 1989; Droser and Li, 2001).

The basal Mount Simon Sandstone is locally dominated by feldspar-rich cobble conglomerate and stratified gravel conglomerate, formed as distal alluvial fan deposits shed from adjacent Precambrian uplands into the proto-Illinois Basin. Poorly sorted sandstone represents terrestrial braided fluvial systems with rare thin laminations of slack water muds without trace fossils. In the upper Mount Simon Sandstone, the occurrence of vertical *Skolithos* trace fossils and lags of inarticulate brachiopods mark the transition to the marginal marine environments. Rare well-sorted sandstone indicates eolian sedimentation in patches within the braided fluvial systems. The interstratified sandstone and shale lithofacies indicate freshwater to brackish deltaic environments that transition to marginal marine environments where *Planolites* trace fossils are found. The shale lithofacies is similar to lithofacies observed within the marine Eau Claire Formation, but contains no trace fossils within the shale and only horizontal *Planolites* within the thin silt and sandstone interbeds. The shale beds commonly have large (5-mm diameter) syndepositional pyrite zones with shale bed compaction surrounding them. This facies is likely the remnant of marginal marine lagoons with restricted circulation and anoxic waters that prevented metazoan activity. Thin interbeds of silt and sandstone may have formed during storm events that temporarily introduced oxygenated waters and allowed vermiform metazoans to leave marine *Planolites* trace fossils.

POROSITY AND DIAGENETIC HETEROGENEITIES

Porosity decrease with depth has been well documented in many sandstones, but the nature of this trend (linear vs. exponential or otherwise) and mechanisms responsible for this decrease vary widely between units. The overall trends in Mount Simon Sandstone porosity have been measured by many workers during the last several decades using petrographic analysis (point counting), core analyses, and estimates from geophysical logs (Metarko, 1980; Hoholick et al., 1984; Shebl, 1985; Makowitz, 2004; Kunledare, 2005; Medina et al., 2011). Our aim with this work is not to reproduce these data, but to describe the character of the porosity and explore the causes for the range in porosity at any given depth. Previous studies have identified porosity trends in the Mount Simon Sandstone as primarily dependent on burial depth, with an exponential decrease with depth related to both physical and chemical compaction (e.g., quartz cementation, pressure solution). However, porosity data show that for a given depth range (e.g., between about 3000 and 4000 ft [~900 and ~1200 m]), a large variability exists from values of 1 to 40% porosity (Figure 6), suggesting that other factors, besides compaction, are important in controlling Mount Simon Sandstone porosity.

Our petrographic image analysis of porosity generally correlates with porosity measured from point counts and porosity derived from core analyses. However, imaged-derived data consistently underestimates porosity compared with core analyses because of the limitations based on epoxy impregnation and image resolution and may be more representative of effective porosity than total porosity (Ehrlich et al., 1984, 1991; Mowers and Budd, 1996; Anselmetti et al., 1998; Cerepi

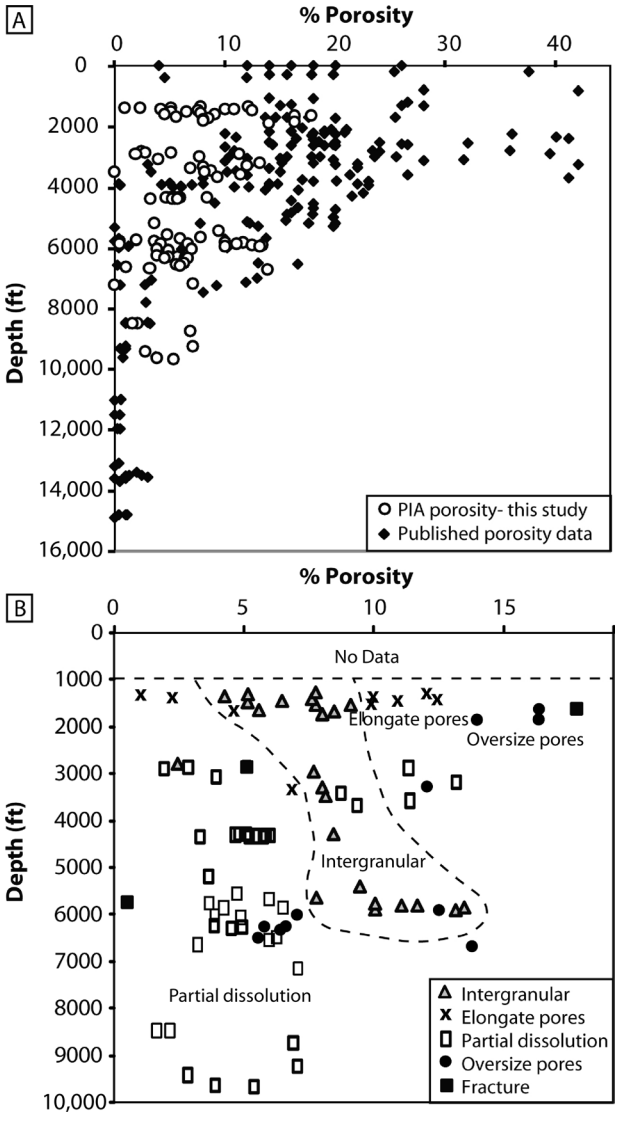

Figure 6. Petrographically derived porosity trends in the Mount Simon Sandstone. (A) Porosity with depth. Plot includes published porosity data compiled from Kunledare (2005), Makowitz (2004), Shebl (1985), Hoholick et al. (1984), and Metarko (1980) (n = 198 total) and petrographic image analysis–derived porosity determined in this study (n = 91). Note large variability in porosity for any given depth range. Porosity data derived from core analysis (i.e., He injection) or well-log data are not included in this plot. (B) Classification of pore types in the same Mount Simon Sandstone samples subject to petrographic image analysis. Five dominant porosity types are recognized, including intergranular porosity, elongate pores, partial dissolution, oversize pores, and fracture porosity. Each sample was classified based on the dominant pore type observed in that thin section. The deepest samples investigated are dominated by dissolution porosity.

et al., 2001). Although we do observe petrographic textures that indicate compaction (e.g., concave-convex and sutured grain contacts, stylolitic textures) and abundant quartz cementation, we do not observe a straightforward relationship between these features, porosity, and depth. The dominant sources of porosity observed in the Mount Simon Sandstone include intergranular porosity, elongate pores, oversize pores, fracture porosity, and dissolution porosity (Figure 6B). Although quartz cementation and compaction may cause a loss of porosity with depth, dissolution of framework and authigenic minerals results in the formation of dissolution porosity at depth. On a single well scale, porosity actually tends to increase with depth (Figure 7). This is likely caused by stratigraphic variations in primary textures, such as grain size and sorting that are associated with transitions in depositional environments from coarser grained facies at the base of the Mount Simon Sandstone to finer grained facies toward the transition into the overlying Eau Claire Formation (Figure 3), as well as stratigraphic changes in the framework grain composition. For example, the lower Mount Simon Sandstone tends to have more feldspar-rich zones, which, in turn, tend to have more framework grain dissolution and increased porosity relative to the feldspar-poor zones higher up in the section (Figure 8).

Previous studies on the diagenetic history of the Mount Simon Sandstone suggest that the unit has been a major paleo-fluid-flow conduit for hydrothermal and chemically complex fluids (Hoholick et al., 1984; Fishman, 1997; Chen et al., 2001). The apparent chemistry, timing, and geologic associations between alterations seen in the Mount Simon Sandstone and economic mineral accumulations (Mississippi Valley–type mineralization) suggest that some of the fluids that have passed through the formation may have been ore-forming brines (Fishman, 1997; Chen et al., 2001). This history of fluid flow illustrates the reservoir potential within the Mount Simon Sandstone. The complex physical and chemical diagenetic history has resulted in variable types of cements (grain coatings, overgrowths, and pore filling) in the formation. The major cements affecting porosity in the Mount Simon Sandstone consist of quartz and feldspar overgrowths, iron-bearing illitic clays, kaolinite, and iron oxides (Figure 9). Specific diagenetic processes related to these groups are described below. Both the composition and the texture of the authigenic minerals in the Mount Simon Sandstone are critical factors in determining the fate of injected CO_2.

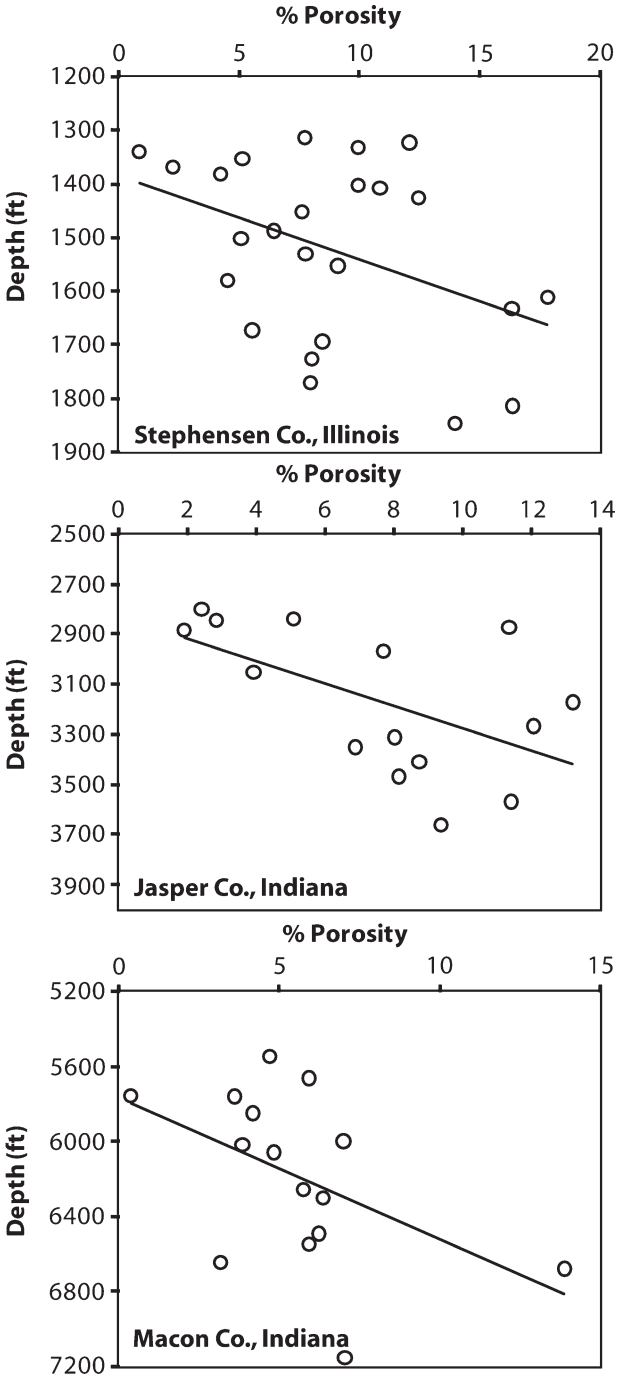

Figure 7. Porosity variations with depth (from petrographic image analysis) for samples from Stephenson Co, Illinois; Jasper Co., Indiana; and Macon Co., Indiana, with a best-fit linear trend line. On individual well scales, porosity tends to increase with depth, in contrast to the basin scale that generally decreases with depth (Figure 6). This is likely a result of multiple factors, including diagenesis and stratigraphic changes in lithology—from more arkosic (e.g., more dissolution porosity) and coarser grained sandstone with higher porosity at the base of the Mount Simon Sandstone to finer grained intervals with more argillaceous material toward the top of the Mount Simon Sandstone.

Quartz

Our petrographic and geochemical results, as well as other Mount Simon Sandstone studies, show that the formation is primarily a quartz arenite composed of a mature quartz grains (as much as ~90–95% quartz) (Figure 10; Table 2) (Hoholick et al., 1984; Fishman, 1997; Barnes et al., 2009). However, our analyses (point-count data and whole-rock major oxide data) show that specific samples can vary in quartz composition from only 5% in shales to 99% total quartz in clean silica-cemented sandstones. Other observed trace detrital grains include zircon, rutile, and chromite. Some quartz grains near the base of Mount Simon Sandstone show etching and large dissolution pits, suggesting that these grains have been corroded by some extreme fluids (Figure 9F2). Quartz overgrowths are the most common cement, and CL microscopy shows that multiple generations of quartz cementation exist (Figure 11). They are seen in both relatively shallow and deep samples (Figure 9C), without a consistent depth-dependant pattern in where they occur. A wide range of conditions could have existed during quartz cementation (Makowitz et al., 2006). McBride (1989) suggests that upward migration of silica-rich fluids will actively precipitate quartz at 140°F (60°C), correlating to a burial depth of approximately 6500 to 9800 ft (~2000–3000 m). Others have modeled abundant quartz cementation to occur at higher temperatures of 194 to 212°F (90–100°C), correlating to a burial depth of about 9840 to 13,100 ft (~3000–4000 m), assuming a thermal gradient of 77 to 86°F/mi (25–30°C/km) (Giles et al., 2000). Although hydrothermal fluid migration may not have been necessary to form quartz cement in the proto-Illinois Basin, fluid inclusion analysis suggests that quartz overgrowths in the Mount Simon Sandstone precipitated from fluids with high salinity and anomalously high temperatures compared with the expected burial temperatures (Fishman, 1997). The observation of quartz overgrowths in shallow samples (Figure 9C2, sample at 1672 ft [506 m]) suggests that either the conditions suitable for quartz cementation existed in this shallow setting or that these cements formed during the time that this part of the basin was buried much deeper. Coal maturation studies suggest that as much as 5000 ft (1524 m) of additional sediment filled the Illinois Basin at its maximum burial (Damberger, 1971), and with these potential maximum burial depths, the high temperatures needed for quartz cementation would be reached without necessitating hydrothermal fluids.

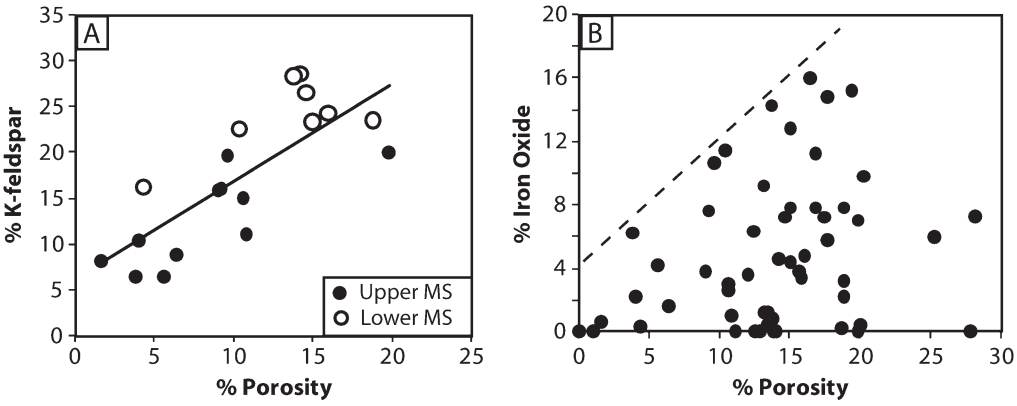

Figure 8. Comparisons between sandstone composition and porosity based on thin-section point-count data on sidewall core and whole-core samples from Macon Co., Illinois (Table 2). (A) Correlation between the amount of K-feldspar and porosity in two densely sampled parts of the formation (two 30-ft [9-m] sections of core; "upper MS" refers to Mount Simon Sandstone samples from 6409 to 6430 ft [1954–1960 m], and "lower MS" refers to Mount Simon Sandstone samples from 6751 to 6773 ft [2058–2065 m]). Both zones are primarily composed of medium-grained sandstone that are otherwise lithologically similar (similar grain size, grain shape, sorting, etc.). (B) Comparison between the amount of iron oxide and porosity. Samples with at least a few percent iron oxide (more than ~4%) have a corresponding minimum porosity (dashed line). Note that there are three outliers with iron oxide compositions above 20%, which are not shown that do not fit this relationship.

Feldspar

The Mount Simon Sandstone contains abundant detrital and early authigenic K-feldspar, like much of the Late Precambrian and early Paleozoic strata of North America (Figures 8, 9, 11, 12) (Buyce and Friedman, 1975; Odom, 1975; Liu et al., 2003). Some intervals of the Mount Simon Sandstone are composed of a feldspathic or subfeldspathic arenite with as much as approximately 40% K-feldspar (Figure 9D2). Whole-rock geochemical data show that K_2O values range from 0.1 to 7.9% and correlate well with increasing Al_2O_3 values, suggesting that the potassium concentrations are related to K-feldspar and clay distribution. In much of the Mount Simon Sandstone, the feldspar grains tend to be very fine grained relative to the quartz grains, and in some areas, appear to be purely authigenic (Figure 9D1). It can be very difficult to distinguish between detrital feldspar grains and feldspar overgrowths with standard transmitted and reflected light petrography. The use of CL microscopy allows for distinction between these two populations (Figure 11) but has not yet been done on a large enough sample swath to allow for quantification of detrital versus authigenic sources. Potential processes responsible for the formation of the authigenic K-feldspar include sediment interaction with hot or low-temperature brines and/or subaerial chemical weathering (Duffin, 1989). It has been suggested that feldspar overgrowths may have formed relatively early in the burial history of the Mount Simon Sandstone and may overlap with primary or secondary events of quartz overgrowth formation (Duffin et al., 1989) (Figure 11C). The depletion of feldspar from upper Precambrian basement has been suggested to be caused by reactions with brines derived from overlying Mount Simon Sandstone (Mensing and Faure, 1983). The diagenetic dissolution of feldspar provides significant porosity to the Mount Simon system and would also result in the formation of diagenetic clays in the pores (Figures 8, 11) (Heald and Larese, 1973). The alteration of feldspar to clay would release silica, which could be a potential source for a generation of quartz cementation.

Backscattered electron micrographs were used to determine the amount of feldspar that lines pores in 25 Mount Simon Sandstone samples from six different wells (Figure 12). The porosities of the samples investigated ranged from less than 2 to more than 18%. The perimeter of individual pores and the length of this perimeter that is occupied by feldspar were measured (Figure 12B, C). These data suggest that a straightforward relationship exists between modal percent feldspar and the percent of feldspar present as pore space linings (Figure 12D). However, the relationship between total percent feldspar and the amount of feldspar lining pores is not 1:1. Instead, a greater amount of feldspar lining the pores is present than the overall feldspar volume percent, suggesting

that some of the feldspar lining the pores are a later forming cement.

Clay Minerals

Clay minerals, although volumetrically minor in most areas, are important factors in determining the reservoir injectivity of the Mount Simon Sandstone. Multiple generations of clays were formed during various stages of the diagenetic history of this unit. These clays greatly influence fluid-flow pathways by blocking pore throats and could potentially be the more reactive phases in a CO_2-saturated system. Clays identified in the Mount Simon Sandstone with spectroscopy and x-ray diffraction include illite group clays (mixed layer illite-smectite, iron-rich illite), kaolinite, and chlorite (Fishman, 1997; Morse and Leetaru, 2005) (Figure 9E, F). The presence of iron-rich clay is also supported by the whole-rock geochemical data (Figure 10A). The source of these clays could include the breakdown of detrital clays and micas. However, most petrographically observed detrital micas are relatively unaltered, suggesting that most clays are derived from the breakdown of feldspars and in-situ authigenic precipitation from paleo-fluids. A close spatial association is seen between weathered feldspar grains and authigenic clays (Figure 11D). Detrital versus authigenic clay origins are interpreted from the morphology of the clays. Clay morphology ranges from ribbon-like textures parallel to bedding for detrital clays to radial and random fibrous grain lining and pore-filling textures in authigenic populations (Figure 9E). Spectral data show that midformation pore-filling kaolinite cement is limited to the central part of the Illinois Basin (Macon Co., Illinois,

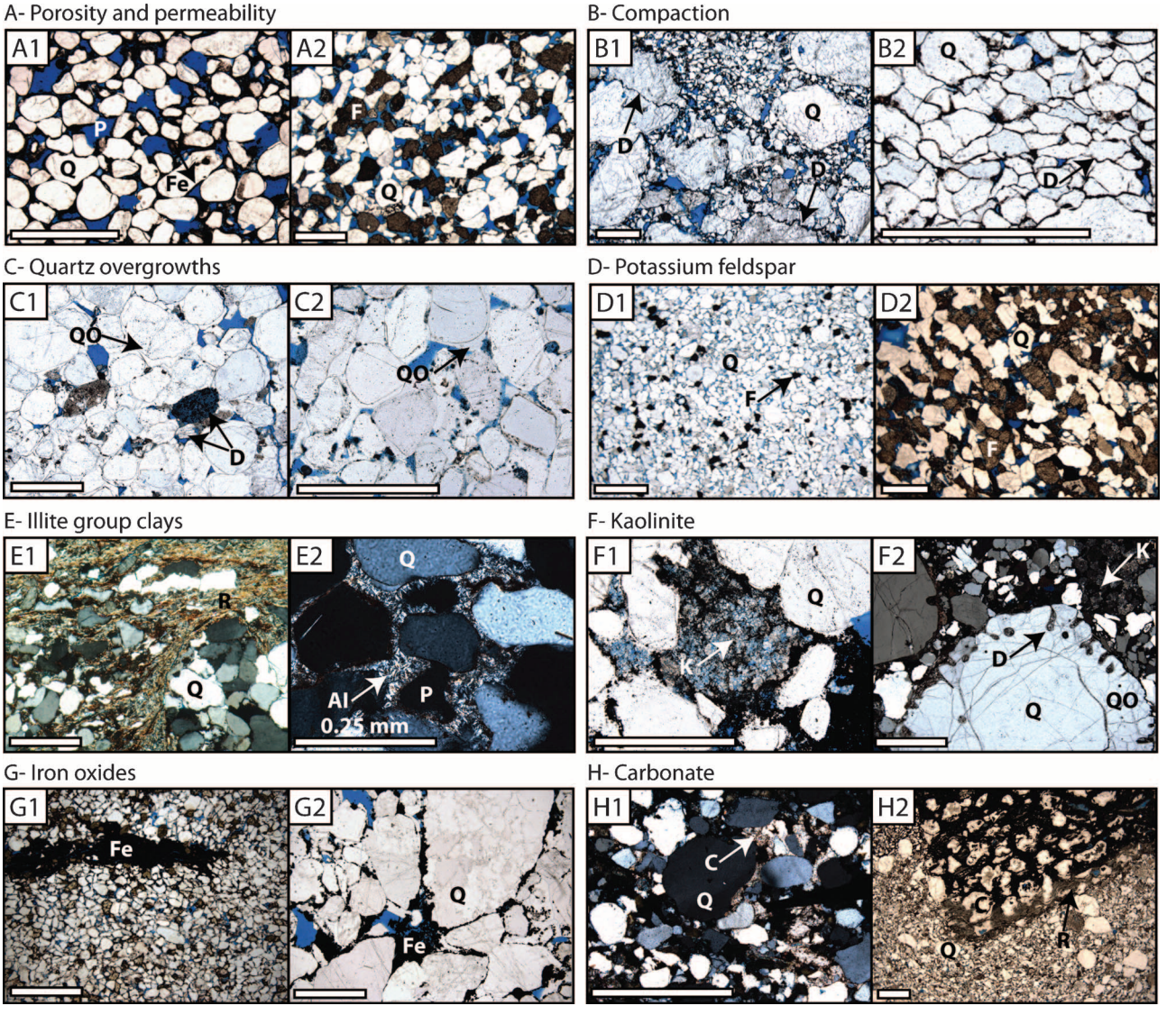

and Champaign Co., Indiana) (Figure 9F1). The basal Mount Simon Sandstone also contains kaolinite just above the Precambrian unconformity, which decreases in abundance upsection (Figure 9F2). This likely reflects either a relict weathering surface related to the unconformity or that paleo-fluids that precipitated kaolinite traveled along this boundary.

Iron Oxides

The Mount Simon Sandstone has experienced significant iron-related diagenesis at multiple points through its burial history. Spectral data show the presence of primarily hematite, but also some goethite in the Mount Simon Sandstone. Petrographic relationships indicate that iron oxide precipitated repeatedly during the burial history of the sandstone. Striking color variations and iron oxide liesegang bands are common throughout the Mount Simon Sandstone. Textural relationships suggest that some of the red coloration was very early and has been subsequently "bleached" by iron-reducing (or low-pH) fluids (Figure 2). Whole-rock geochemical analyses show that the red sandstone zones contain an average of 2.1 wt. % iron oxide, whereas the white zones contain 1.3 wt. % iron oxide, but some samples can contain as much as about 10 wt. % iron oxide (Figure 10). Although some of this measured iron is likely associated with clays (Figure 10A), a separate population of red sandstone samples shows an increase in Fe without the corresponding increase in Al (Figure 10A inset). These are interpreted as samples with iron oxide cements that are not associated with clays. Point-count data show that some samples are composed of more than 20% iron oxide. However, the exact nature of these minerals and mixtures with clay can be difficult to distinguish petrographically. Various morphologies of iron oxides are observed, including grain coatings (Figure 9G2) and apparent "displacive" patches (Figure 9G1) that may be altered remnants of early diagenetic pyrite. Where iron oxide grain coatings are observed, there tends to be little to no quartz cementation and relatively high porosity (Figures 8B, 9A1). The iron oxides may have acted to preserve primary porosity by inhibiting the precipitation of quartz overgrowths. In contrast, more dense accumulations of pore-filling iron oxide cement greatly reduce the available pore space and acted as barriers to further fluid flow.

Other Authigenic Phases

Other authigenic mineral phases occur locally throughout the Mount Simon Sandstone and are volumetrically

Figure 9. Petrographic examples of detrital and diagenetic characteristics that influence reservoir quality. All scale bars 1 mm across (except for E2). Samples are vacuum impregnated with blue epoxy and stained for K-feldspar (brown stain). All micrographs were taken in plane light unless otherwise noted. Annotations on micrographs: Q = quartz grains; F = feldspar; P = porosity; D = dissolution; QO = quartz overgrowth cementation; R = ribbon-like micas or clays; AI = authigenic illite; K = kaolinite; Fe = iron oxide; C = carbonate. (A) High porosity and permeability. (A1) Iron oxide grain coatings inhibit cement growth and preserve primary porosity in a well-sorted, well-rounded, fine- to medium-grained sandstone; Macon Co., Illinois, 6000 ft (1829 m), 20% porosity, 323 md permeability. (A2) High primary porosity as well as significant feldspar content that results in dissolution porosity in medium-grained sandstone; Champaign Co., Illinois, 5836 ft (1779 m), 23% porosity, 1280 md permeability. (B) Physical and chemical compaction. (B1) Very coarse sandstone with stylolitic compaction texture; Knox Co, Indiana, 8633 ft (2631 m). (B2) Fine-grained sandstone with sutured grain contacts; LaGrange Co., Indiana, 4306 ft (1312 m). (C) Quartz overgrowths from deep (C1) and shallow (C2) samples. (C1) Medium-grained sandstone with significant quartz cement and feldspar dissolution; Knox Co, Indiana, 9617 ft (2931 m). (C2) Fine-grained sandstone with quartz overgrowths from approximately 8000 ft (2438 m) shallower burial depth than the sample shown in (C1); Stephenson Co., Illinois, 1672 ft (510 m). (D) Potassium feldspar (stained dark yellow-brown) variability. (D1) Fine-grained sandstone with very fine regularly distributed K-feldspar grains that are likely authigenic; Champaign, Illinois, 5425 ft (1654 m). (D2) Medium-grained sandstone with a major component of both detrital and authigenic K-feldspar; Macon, Illinois, 6928 ft (2112 m). (E) Illite group clays (illite, interstratified illite/smectite, Fe-rich illite, mica, etc.). (E1) Fine-grained sandstone with ribbon-like pore-filling Fe-rich illite; LaGrange Co, Indiana, 4326 ft (1319 m), cross-polarized light. (E2) Fine-grained sandstone with fibrous radial illite coating grains and projecting into pore space; Laporte Co., Indiana, 3063 ft (934 m), cross-polarized light, scale bar = 0.25 mm, porosity not embedded with blue epoxy in this sample. (F) Kaolinite cements. (F1) Coarse-grained sandstone with kaolinite cement; Champaign Co., Illinois, 6500 ft (1982 m). (F2) Quartz granule with kaolinite cement filling dissolution pits and as an intergranular cement; Macon Co., Illinois, 7148 ft (2179 m), cross-polarized light. (G) Iron oxide cements. (G1) Very fine grained sandstone with displacive iron oxide cement; LaGrange Co., Indiana, 4309 ft (1313 m). (G2) Very coarse grained sandstone with iron oxide cement that postdates quartz cement; Champaign Co., Illinois, 6111 ft (1863 m). (H) Carbonates. (H1) Fine-grained sandstone with intergranular calcite cement; Jasper Co., Indiana, 2885 ft (879 m), cross-polarized light. (H2) Very fine grained sandstone with large carbonate and clay-rich bioclast; Macon Co., Illinois, 6852 ft (2089 m).

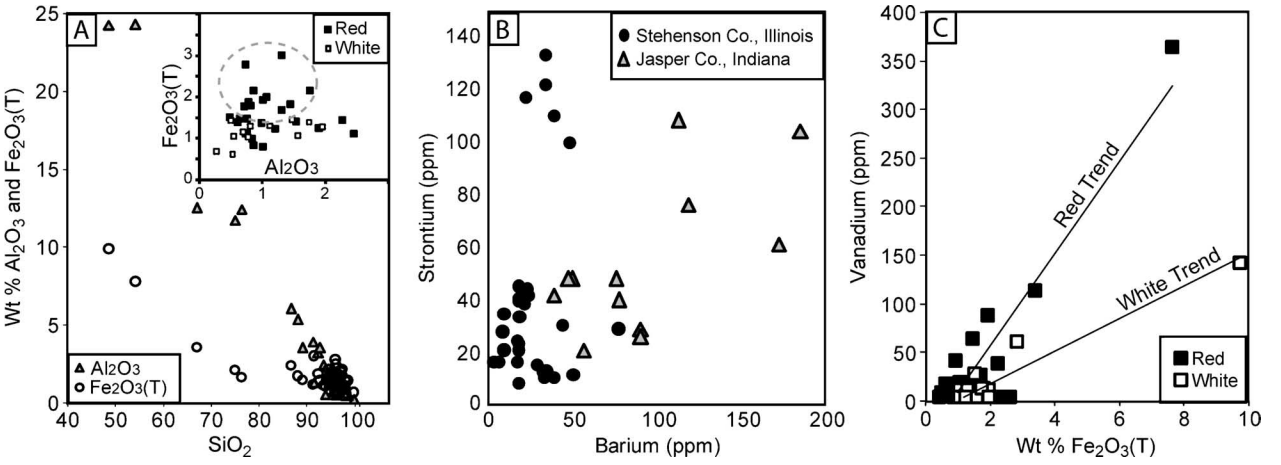

Figure 10. Examples of major oxide and trace elements variations in the Mount Simon Sandstone measured with whole-rock chemical analyses (n = 51, includes representative samples that span entire sections in Stephenson Co., Illinois, and upper half of formation in Jasper Co., Indiana; Table 2). (A) Total Si versus Fe and Al concentrations showing distinct Al-rich and Fe-rich populations. Samples with corresponding elevated Fe and Al likely represent iron-bearing clays (dark-red mud drapes). The population of samples with elevated Fe that does not correspond to elevated Al likely represents iron oxide–enriched sandstone (inset). (B) Spatial difference between cores in the concentration of Ba versus Sr. In general, the samples from Jasper Co. have higher Ba than those from Stephenson Co., and both cores have a few high Sr samples that span the depths collected and are not associated with a specific stratigraphic horizon. These data suggest that these areas either have differences that reflect a provenance signature (with potentially more depositional barite associated with the more eastern Jasper Co. system) or that these areas have experienced the influence of different diagenetic fluids. (C) Concentration of vanadium, associated with increased amounts of iron oxide. This trend is seen in samples from both Stephenson and Jasper Co. and tends to be most pronounced in red samples compared with white samples, suggesting that the V is adsorbed onto pigment-producing iron oxides rather than iron-bearing clays present in the white samples. Trace metals commonly adsorb onto iron oxides and could potentially be released if the iron oxides were dissolved.

significant in some intervals or areas. For example, both detrital and authigenic carbonates occur within the unit (Figure 9H) and are associated with the gradational contact with the overlying carbonate-rich Eau Claire Formation (Figure 4). Mineralogical data show the presence of both dolomite and calcite, and some carbonates are observed as isolated biogenic clasts within the otherwise dominantly siliciclastic unit (Figure 9H2). Other relatively minor but locally important authigenic cements include gypsum, pyrite, anhydrite, barite, and fluorite (Fishman, 1997). Spatially distinct trace element concentrations of barium may be remnants of

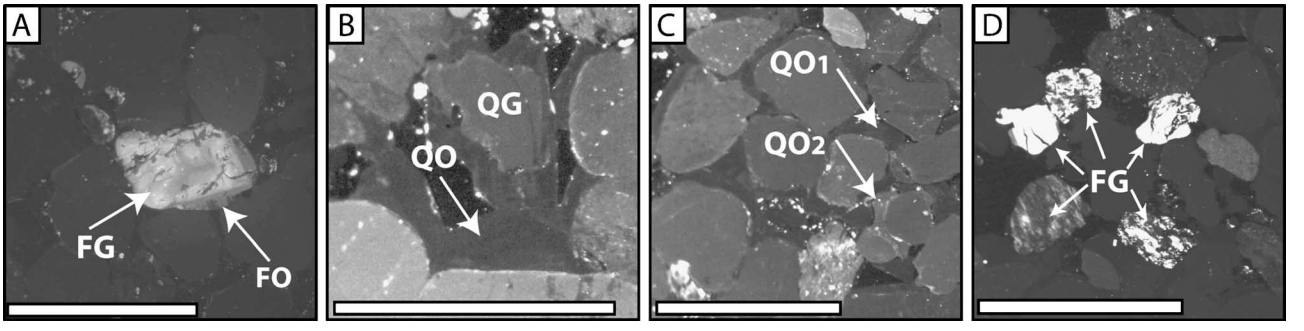

Figure 11. Cathodoluminescence (CL) microscopy images of the Mount Simon Sandstone. All examples from medium-grained sandstone samples from Macon Co., Illinois, 6867 ft (2094 m). Scale bars = 1 mm. (A) Example of CL differentiation between detrital (FG) and authigenic (FO) feldspar in a medium-grained sandstone. (B) Quartz overgrowths (QO) surrounding detrital quartz grains. (C) Multiple generations of quartz cement (based on variable CL "brightness" labeled QO1 and QO2). (D) Detrital feldspar grains (bright) with variable amounts of intragranular dissolution, weathering, and associated clays.

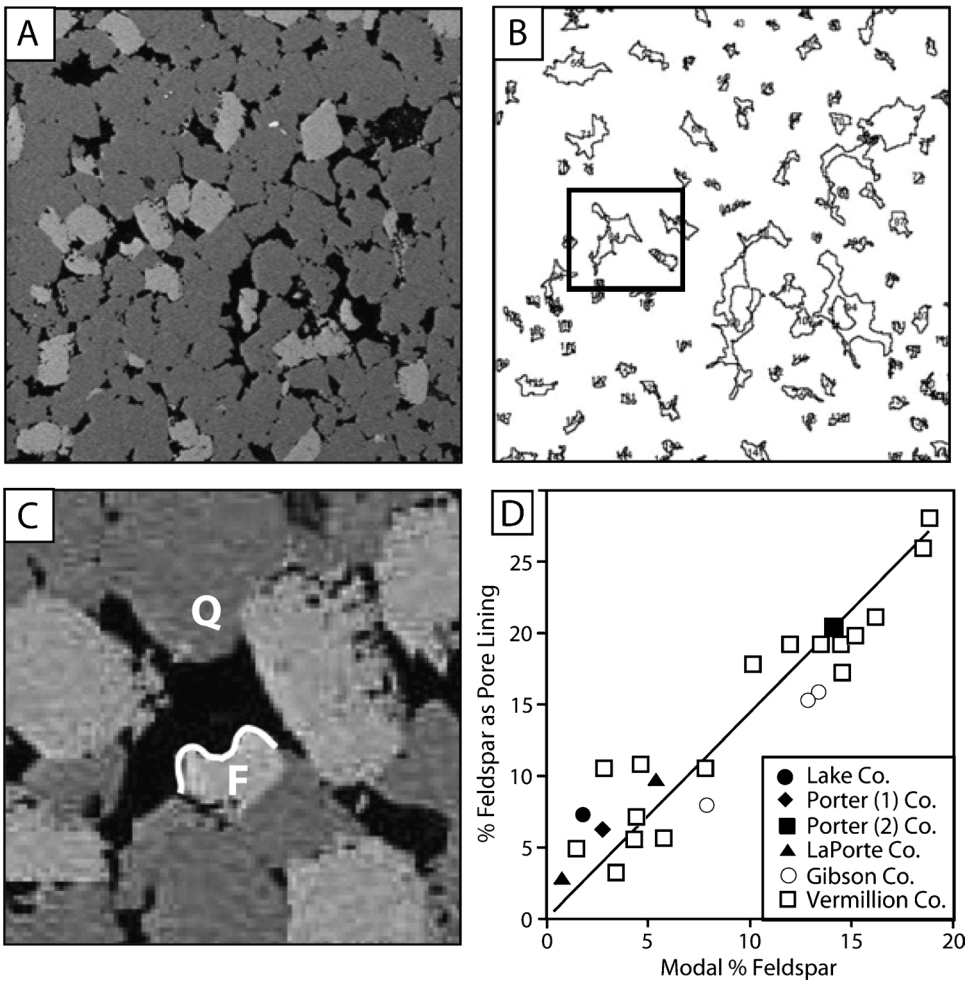

Figure 12. Analysis of the percent of the large pore perimeters lined by feldspar compared with the total feldspar for selected Mount Simon Sandstone samples from Lake Co., Indiana; Vermillion Co., Indiana; and Gibson Co., Indiana. (A) Backscattered electron image showing the pore spaces (black), quartz grains with overgrowths (dark gray), and feldspar grains with overgrowths (light gray). Image is 1 mm across. (B) ImageJ generated map showing the perimeters of individual pore spaces polygons (n = 152). ImageJ simultaneously measures the surface area and perimeter length of each pore. (C) Close-up view of a single pore space that is lined by both quartz and feldspar. For individual pores, the part of that perimeter that is occupied by feldspar is manually traced to allow for calculation of the percentage of pore space that is lined by feldspar (solid white line). The total length of the lining that is made up of feldspar is then subtracted from the total perimeter length, thus permitting one to determine the relative proportions of quartz and feldspar that make up the entire pore space lining. (D) The relationship between modal percent feldspar in the 25 samples analyzed, and percent feldspar as pore space lining. Also shown is a linear regression through the data that has a good correlation coefficient (R^2) of 0.94.

dissolved barite in the northeastern part of the basin (Figure 10B).

DISCUSSION

Implications for Fluid Flow and Mineral Reactivity in a CO_2 System

Petrophysical calculations have estimated the Mount Simon Sandstone to have the potential to store up to 355 GT of CO_2 in the midwest region (Medina et al., 2011). Depositional and diagenetic heterogeneities are major factors in determining potential fluid-flow pathways, the amount of porosity available for sequestration, and the types of minerals that are in contact with pore space and may be reactive in a CO_2 system.

The depositional facies in the Mount Simon Sandstone will influence patterns of fluid flow and potential CO_2 migration. Primary depositional flow barriers in the Mount Simon Sandstone consist of isolated overbank mudstones interbedded within braided channel

deposits, interbedded mudstone and sandstone resulting from tidal influence, and the interbedded mudstone and siltstone referred to as the "B-cap" (Figure 4) (Becker et al., 1978). In vegetated braided fluvial systems, overbank and flood-plain deposits can be of a great enough extent to cause large vertical flow baffles and compartmentalization of horizontal flow, but in a pre-vegetative Cambrian system, the scarcity of fine-grained materials limited the formation of large-scale flow barriers (Long, 2006; Millson et al., 2008). Overbank deposits are local in scale and would not act as a barrier to horizontal flow. However, these thin mudstone layers would act as a baffle to vertical flow, slowing the rise of buoyant fluids to the seal (Leetaru et al., 2008; Millson et al., 2008). Similarly, mudstones that were deposited because of tidal processes will also be local in scale and not a strong inhibitor to horizontal flow. The B-cap is only seen in northern Indiana and is not a regionally extensive vertical flow barrier.

The Mount Simon Sandstone contains both detrital and authigenic mineral phases that could potentially be reactive in a CO_2 system. Mineral dissolution rates are several orders of magnitude higher at low pH (pH of ~3 or 4) that would be expected in a CO_2 system and would cause the formation brines to become undersaturated with respect to minerals such as carbonates, aluminosilicates, and iron oxides that are present in the reservoir sandstone (Kharaka et al., 2006). Carbonate minerals would be highly reactive in a CO_2-generated acid brine. Although isolated zones of carbonate grains and cements exist (Figure 9H; Table 2), they are only consistently seen at the top of the Mount Simon Sandstone in the transition with the Eau Claire Formation (Figure 4). If dissolved, carbonates could potentially provide important ions for the formation of long-term carbon-sequestering mineral phases.

Zones in the Mount Simon Sandstone with abundant feldspar present some of the best reservoir characteristics (Figure 8), but also present an abundance of potentially reactive surfaces. The amount of feldspar lining pores is greater than the overall amount of feldspar in the rocks (Figure 12), which implies that more reactive feldspar mineral surfaces are available for potential reactions with CO_2 filling the pores than would be indicated by the total volume percent feldspar in the rock.

The Mount Simon Sandstone contains authigenic iron oxide, iron oxyhydroxide phases, and also iron-bearing clay minerals (e.g., Fe-rich illites, chlorite). The presence of these iron-rich minerals has significant implications for the types of changes that could occur within this reservoir with large-scale CO_2 storage. Geochemical modeling shows that the pH of formation brines can drop significantly, even with the type of high-salinity conditions that exist in the Illinois Basin (Parry et al., 2007). The expected drop in pH related to CO_2 injection could cause dissolution of the iron-bearing minerals, potentially mobilizing associated trace metals that are commonly adsorbed onto iron oxides (e.g., vanadium; Figure 10C) or organic compounds (Palandri and Kharaka, 2005; Kharaka et al., 2006). Understanding the potential for dissolution of minerals in the reservoir is significant because the possibility of eventual precipitation of carbonate minerals capable of trapping CO_2 over geologic time scales depends on the availability of cations that would be provided by dissolution of these mineral precursors (Xu et al., 2004; Peters, 2009).

Future Work

Ongoing large-scale CO_2 sequestration demonstrations focused on the Mount Simon Sandstone will require careful characterization research on compositional and textural variability in this important reservoir before, during, and after CO_2 injection. The availability of new cores of Mount Simon Sandstone will allow us to expand our understanding of this unit and the spatial variability of depositional facies, petrologically distinct subbasins, and patterns of diagenetic modification. Ongoing and future work will include more detailed scanning electron microscopy and energy dispersive x-ray analysis focused on specific authigenic phases and pore characteristics, use of CL to quantify percentage of authigenic versus detrital quartz and feldspar, and experimental evaluation of the effects of exposure to CO_2-charged brines under elevated pressure and temperature conditions. These studies will provide important inputs for reactive transport modeling, fluid-flow modeling, fluid pressure modeling and will allow for baseline comparisons after injection has ensued.

CONCLUSIONS

Sedimentologic, petrographic, geochemical, and mineralogical analyses of the Mount Simon Sandstone demonstrate the reservoir variability that occurs throughout

this formation as a result of spatially complex depositional and diagenetic processes. This unit has great potential as a reservoir for CO_2, but realization of the maximum possible storage capacity requires detailed understanding of the textural and mineralogical variability that will influence the fate of injected CO_2. Porosity variations do not exhibit a simple relationship with depth, but are related to stratigraphic transitions in depositional facies and regional patterns in both porosity-enhancing (e.g., K-feldspar dissolution, iron oxide grain coatings) and porosity-destroying (e.g., quartz overgrowths, clay precipitation) processes. This study provides a background framework for identifying and evaluating this heterogeneity. As new cores related to ongoing CO_2 sequestration efforts become available, future work will continue to map out specific depositional and diagenetic facies and further quantify specific compositional patterns. Our analysis suggests that, in addition to depositional facies, burial depth, and primary detrital components, the specific diagenetic processes and authigenic mineral phases present in the formation are important factors in reservoir quality and will influence the fate of injected CO_2.

REFERENCES CITED

Anselmetti, F. S., S. Luthi, and G. P. Eberli, 1998, Quantitative characterization of carbonate pore systems by digital image analysis: AAPG Bulletin, v. 82, p. 1815–1836.

Barnes, D. A., D. H. Bacon, and S. R. Kelley, 2009, Geological sequestration of carbon dioxide in the Cambrian Mount Simon Sandstone: Regional storage capacity, site characterization, and large-scale injection feasibility, Michigan Basin: Environmental Geosciences, v. 16, p. 163–183, doi:10.1306/eg.05080909009.

Becker, L. E., A. J. Hreha, and T. A. Dawson, 1978, Pre-Knox (Cambrian) stratigraphy in Indiana: State of Indiana Department of Natural Resources Geological Survey, 72 p.

Benson, S. M., and D. R. Cole, 2008, CO_2 sequestration in deep sedimentary formations: Elements, v. 4, p. 325–331, doi:10.2113/gselements.4.5.325.

Bowen, B. B., B. A. Martini, M. A. Chan, and W. T. Parry, 2007, Reflectance spectroscopic mapping of diagenetic heterogeneities and fluid-flow pathways in the Jurassic Navajo Sandstone: AAPG Bulletin, v. 91, p. 173–190, doi:10.1306/08220605175.

Buyce, M. R., and G. M. Friedman, 1975, Significance of authigenic K-feldspar in Cambrian-Ordovician carbonate rocks of the Proto-Atlantic shelf in North America: Journal of Sedimentary Petrology, v. 45, p. 808–821.

Cant, D. J., and F. J. Hein, 1986, Depositional sequences in ancient shelf sediments: Some contrasts in style: Shelf Sands and Sandstones, v. 2, p. 303–312.

Cerepi, A., L. Humbert, and R. Burlot, 2001, Petrophysical properties of porous medium from petrographic image analysis data: Colloids and Surfaces, v. 187–188, p. 233–256.

Chen, Z., L. R. Riciputi, C. I. Mora, and N. S. Fishman, 2001, Regional fluid migration in the Illinois basin: Evidence from in-situ oxygen isotope analysis of authigenic K-feldspar and quartz from the Mount Simon Sandstone: Geology, v. 29, p. 1067–1070, doi:10.1130/0091-7613(2001)029<1067:RFMITI>2.0.CO;2.

Clark, R. N., 1999, Spectroscopy of rocks and minerals, and principles of spectroscopy, *in* A. N. Rencz, ed., Remote sensing for the earth sciences: Manual of remote sensing: New York, John Wiley and Sons, v. 3, p. 3–58.

Clark, R. N., and T. L. Roush, 1984, Reflectance spectroscopy: Quantitative analysis techniques for remote sensing applications: Journal of Geophysical Research, v. 89, p. 6329–6340, doi:10.1029/JB089iB07p06329.

Damberger, H. H., 1971, Coalification patterns of the Illinois Basin: Economic Geology, v. 66, p. 488–494, doi:10.2113/gsecongeo.66.3.488.

Dott, R. H., C. W. Byers, G. W. Fielder, S. R. Stenzel, and K. E. Winfree, 1986, Aeolian to marine transition in Cambro–Ordovician cratonic sheet sandstones of the northern Mississippi Valley, U.S.A.: Sedimentology, v. 33, p. 345–367, doi:10.1111/j.1365-3091.1986.tb00541.x.

Driese, S. G., C. W. Byers, and R. H. Dott, 1981, Tidal deposition in the basal Upper Cambrian Mt. Simon Formation in Wisconsin: Journal of Sedimentary Petrology. v. 51, p. 0367–0381.

Droser, M. L., and D. J. Bottjer, 1989, Ichnofabric of sandstones deposited in high-energy nearshore environments: Measurement and utilization: Palaios, v. 4, p. 598–604, doi:10.2307/3514750.

Droser, M. L., and X. Li, 2001, The Cambrian radiation and the diversification of sedimentary fabrics, *in* A. Y. Zhuravlev and R. Riding, eds., The ecology of the Cambrian radiation: New York, Columbia University Press, p. 137–164.

Duffin, M. E., 1989, Nature and origin of authigenic K-feldspar in the Precambrian basement rocks of North American midcontinent: Geology, v. 17, p. 765–768, doi:10.1130/0091-7613(1989)017<0765:NAOOAK>2.3.CO;2.

Duffin, M. E., M. Lee, G. K. Klein, and R. L. Hay, 1989, Potassic diagenesis of Cambrian sandstones and Precambrian granitic basement in UPH-3 deep hole, Upper Mississippi Valley, U.S.A.: Journal of Sedimentary Petrology, v. 59, no. 5, p. 848–861.

Ehrlich, R., S. K. Kennedy, S. J. Crabtree, and R. L. Cannon, 1984, Petrographic image analysis: I. Analysis of reservoir pore complexes: Journal of Sedimentary Petrology, v. 54, p. 1365–1378.

Ehrlich, R., S. J. Crabtree, K. O. Horkowitz, and J. P. Horkowitz, 1991, Petrography and reservoir petrophysics: I. Objective classification of reservoir porosity: AAPG Bulletin, v. 75, p. 1547–1562.

Fischietto, N. E., 2009, Lithofacies and depositional environments of the Cambrian Mount Simon Sandstone in the northern Illinois Basin: Implications for CO_2 sequestration: Master's thesis, Purdue University, West Lafayette, Indiana, 114 p.

Fishman, N. S., 1997, Basinwide fluid movement in a Cambrian paleoaquifer: Evidence from the Mt. Simon Sandstone, Illinois and Indiana, *in* I. P. Montañez, J. M. Gregg, and K. L. Shelton, eds., Basinwide diagenetic patterns: Integrated petrologic, geochemical, and hydrologic considerations: SEPM Special Publication 57, p. 221–234.

Friedmann, S. J., 2007, Geological carbon dioxide sequestration: Elements, v. 3, p. 179–184, doi:10.2113/gselements.3.3.179.

Giles, M. R., S. L. Indrelid, G. V. Beynon, and J. Amthor, 2000, The origin of large-scale quartz cementation: Evidence from large data sets and coupled heat-fluid mass transport modeling, *in* R. H. Worden and S. Morad, eds., Quartz cementation in sandstone: International Association of Sedimentologists Special Publication 29, p. 21–38.

Hagadorn, J. W., R. H. Dott, and D. Damrow, 2002, Stranded on a late Cambrian shoreline: Medusae from central Wisconsin: Geology, v. 30, no. 2, p. 147–150, doi:10.1130/0091-7613(2002)030<0147:SOALCS>2.0.CO;2.

Heald, M. T., and R. E. Larese, 1973, The significance of the solution of feldspar in porosity development: Journal of Sedimentary Petrology, v. 43, p. 458–460.

Hoholick, J. D., T. Metarko, and P. E. Potter, 1984, Regional variations of porosity and cement: St. Peter and Mount Simon sandstones in Illinois Basin: AAPG Bulletin, v. 68, no. 6, p. 753–764.

Holloway, S., 2001, Storage of fossil fuel derived carbon dioxide beneath the surface of the Earth: Annual Review of Energy and the Environment, v. 26, p. 145–166.

Houseknecht, D. W., and F. G. Ethridge, 1978, Depositional history of the Lamotte Sandstone of southeastern Missouri: Journal of Sedimentary Petrology, v. 48, p. 575–586.

Kharaka, Y. K., D. R. Cole, S. D. Hovorka, W. D. Gunter, K. G. Knauss, and B. M. Freifeld, 2006, Gas-water-rock interactions in Frio Formation following CO_2 injection: Implications for the storage of greenhouse gases in sedimentary basins: Geology, v. 34, p. 577–580, doi:10.1130/G22357.1.

Kolata, D. R., and W. J. Nelson, 1991, Tectonic history of the Illinois Basin, *in* M. W. Leighton, D. R. Kolata, D. F. Oltz, and J. J. Eidel, eds., Interior Cratonic basins: AAPG Memoir 51, p. 263–285.

Kunledare, M. A., 2005, Petrographic investigation into the development of secondary porosity in sandstones: A case study of the Cambrian Mount Simon and Galesville Sandstones, Illinois Basin: Ph.D. thesis, University of Missouri-Rolla, Rolla, Missouri, 199 p.

Leetaru, H. E., and J. H. McBride, 2009, Reservoir uncertainty, Precambrian topography, and carbon sequestration in the Mt. Simon Sandstone, Illinois Basin: Environmental Geosciences, v. 16, p. 1–9, doi:10.1306/eg.08110808003.

Leetaru, H. E., S. Frailey, D. Morse, R. J. Finley, J. Rupp, J. A. Drahozval, and J. H. McBride, 2008, Carbon sequestration in the Mt. Simon Sandstone saline reservoir, *in* M. Grobe, J. C. Pashin, and R. L. Dodge, eds., Carbon dioxide sequestration in geological media: State of the science: AAPG Studies 59, p. 1–17.

Lehmann, D. F., N. M. Jones, M. J. and Neese, 2001, Early terrestrial trace fossils from the Upper Ordovician, Bald Eagle Sandstone of Pennsylvania (abs.): Geological Society of America Abstracts with Programs, v. 33, p. 28.

Liu, J., R. L. Hay, A. Deino, and T. K. Kyser, 2003, Age and origin of authigenic K-feldspar in uppermost Precambrian rocks in the North American mid-continent: Geological Society of America Bulletin, v. 115, p. 422–433, doi:10.1130/0016-7606(2003)115<0422:AAOOAK>2.0.CO;2.

Long, D. G. F., 2006, Architecture of prevegetation sandy-braided perennial and ephemeral river deposits in the Paleoproterozoic Athabasca Group, northern Saskatchewan, Canada, as indicators of Precambrian fluvial style: Sedimentary Geology, v. 190, p. 71–95, doi:10.1016/j.sedgeo.2006.05.006.

Makowitz, A., 2004, The genetic association between brittle deformation and quartz cementation elucidated by scanned cathodoluminescence imaging: Ph.D. thesis, The University of Texas at Austin, Austin, Texas, 298 p.

Makowitz, A., R. H. Lander, and K. Milliken, 2006, Diagenetic modeling to assess the relative timing of quartz cementation and brittle grain processes during compaction: AAPG Bulletin, v. 90, p. 873–885, doi:10.1306/12190505044.

McBride, E. F., 1989, Quartz cement in sandstones: A review: Earth Science Reviews, v. 26, p. 69–112, doi:10.1016/0012-8252(89)90019-6.

Medina, C. R., and J. Rupp, 2010, Reservoir characterization and lithostratigraphic division of the Mount Simon Sandstone: Implications for estimations of geologic sequestration storage capacity: AAPG Eastern Section Meeting, September 2010, Kalamazoo, Michigan.

Medina, C. R., J. Rupp, and D. A. Barnes, 2011, Effects of reduction in porosity and permeability with depth on storage capacity and injectivity in deep saline aquifers: A case study from the Mount Simon Sandstone aquifer: International Journal of Greenhouse Gas Control, v. 5, p. 146–156, doi:10.1016/j.ijggc.2010.03.001.

Mensing, T. M., and G. Faure, 1983, Identification and age of neoformed Paleozoic feldspar (adularia) in a Precambrian basement core from Scioto County, Ohio, U.S.A.: Contributions to Mineralogy and Petrology, v. 82, p. 327–333, doi:10.1007/BF00399710.

Metarko, T. A., 1980, Porosity, water chemistry, cement and grain fabric with depth in the upper Cambrian Mount Simon and Lamotte sandstones of the Illinois Basin: Master's thesis, University of Cincinnati, Cincinnati, Ohio, 88 p.

Millson, J. A., J. G. Quin, E. Idiz, P. Turner, and A. Al-Harthy, 2008, The Khazzan gas accumulation, a giant combination trap in the Cambrian Barik Sandstone Member, Sultanate of Oman: Implications for Cambrian petroleum systems and reservoirs: AAPG Bulletin, v. 92, p. 885–917, doi:10.1306/02210807100.

Morse, D. G., and H. E. Leetaru, 2005, Reservoir Characterization and three-dimensional models of Mt. Simon Gas storage fields in the Illinois Basin: Illinois State Geological Survey Circular 567, 72 p.

Mowers, T. T., and D. A. Budd, 1996, Quantification of porosity and permeability reduction due to calcite cementation using computer-assisted petrographic image analysis techniques: AAPG Bulletin, v. 80, p. 309–322.

Odom, I. E., 1975, Feldspar-grain size relations in Cambrian arenites, Upper Mississippi Valley: Journal of Sedimentary Petrology, v. 45, no. 3, p. 636–650.

Ojakangas, R. W., 1963, Petrology and sedimentology of the Upper Cambrian Lamotte Sandstone in Missouri: Journal of Sedimentary Petrology, v. 33, p. 860–873.

Palandri, J. L., and Y. K. Kharaka, 2005, Ferric iron-bearing sediments as a mineral trap for CO_2 sequestration: Iron reduction using sulfur-bearing waste gas: Chemical Geology, v. 217, p. 351–364, doi:10.1016/j.chemgeo.2004.12.018.

Parry, W. T., C. B. Forster, J. P. Evans, B. B. Bowen, and M. A. Chan, 2007, Geochemistry of CO_2 sequestration in the Jurassic Navajo Sandstone, Colorado Plateau, Utah: Environmental Geosciences, v. 14, p. 91–109, doi:10.1306/eg.07120606004.

Peters, C. A., 2009, Accessibilities of reactive minerals in consolidated sedimentary rock: An imaging study of three sandstones: Chemical Geology, v. 265, p. 198–208, doi:10.1016/j.chemgeo.2008.11.014.

Pratt, B. R., 1998, Syneresis cracks: Subaqueous shrinkage in argillaceous sediments caused by earthquake-induced dewatering: Sedimentary Geology, v. 117, p. 1–10, doi:10.1016/S0037-0738(98)00023-2.

Shebl, M. A.-A., 1985, The relation of sandstone diagenesis to petrology and depth: The Mt. Simon, St. Peter, and Aux Vases Sandstones, subsurface, Illinois Basin: Master's thesis, Southern Illinois University at Carbondale, Illinois, 160 p.

Sloss, L. L., 1963, Sequences in the cratonic interior of North America: Geological Society of America Bulletin, v. 74, p. 93–113, doi:10.1130/0016-7606(1963)74[93:SITCIO]2.0.CO;2.

Soegaard, K., and K. A. Eriksson, 1989, Origin of thick, first-cycle quartz arenite successions: Evidence from the 1.7 Ga Ortega Group, northern New Mexico: Precambrian Research, v. 43, p. 129–141.

Tomescu, A. M. F., 2004, Late Ordovician–Early Silurian terrestrial biotas of Virginia, Ohio, and Pennsylvania: An investigation

into the early colonization of land: Ph.D. thesis, Ohio University, Athens, Ohio, 284 p.

Wickstrom, L. H., E. R. Venteris, E. R. Slucher, K. M. Carter, J. McDonald, J. A. Rupp, S. F. Greb, G. R. Baum, W. B. Harrison, and M. B. Hohn, 2006, Geologic storage options and capacities for carbon dioxide sequestration in the Midwest Regional Carbon Sequestration Partnership (MRCSP): Proceedings of the 5th Annual Conference on Carbon Capture and Sequestration, Alexandria, Virginia, May 8–11, 2006, 23 p.

Wigand, M., J. W. Carey, H. Schutt, E. Spangenberg, and J. Erzinger, 2008, Geochemical effects of CO_2 sequestration in sandstones under simulated in situ conditions of deep saline aquifers: Applied Geochemistry, v. 23, p. 2735–2745, doi:10.1016/j.apgeochem.2008.06.006.

Xu, T., J. A. Apps, and K. Pruess, 2004, Numerical simulation of CO_2 disposal by mineral trapping in deep aquifers: Applied Geochemistry, v. 19, p. 917–936, doi:10.1016/j.apgeochem.2003.11.003.